Chapter 3

SoC Estimation of Li-ion Battery and Development of HESS for HEV Applications

In HEVs, battery is a very important and costly equipment. The power available in this battery at any instant can be determined using its state of charge (SoC). This chapter is divided into two parts the part-1 discuss about the SoC estimation of a Lithium-ion battery and part-2 discuss the development of HESS.

***The part-1** presents an effective method to estimate the SoC of a Lithium-ion battery. The values of the RC pairs have been calculated mathematically by solving the circuit model, based on charging and discharging dynamics of the battery. The SoC of the battery is estimated using the combination of coulomb counting and open-circuit voltage methods to minimize the error in estimation.*

The obtained SoC is further corrected for errors using ANFIS based algorithms. The effect of temperature has also been accounted while modelling the battery and in SoC estimation. These obtained SoCs for 3 cases, i.e., without RC/with RC pairs and then tuned with ANFIS based optimization are compared for the same load. The parameter calculation method adopted here results in an efficient and accurate model that keeps track of correct battery SoC. The complete system is validated in real-time using hardware-in-the-loop laboratory setup.

***The part- 2** presents a fully active series-parallel HESS topology which uses a set of UCs deployed in conjunction with the batteries. UCs provide the advantage of quick and frequent charging/discharging without degrading the battery state of health (SoH) and are also used to absorb most of the energy generated due to regenerative braking.*

The major source of energy is Li-ion cells which provide the energy required to run the vehicle whereas the UCs will provide above-average energy required by the motor.

A power-based method to find the specifications of UCs and batteries is described which provides specifications for ESS hybridization.

This method reduces the above-average peaks of the required current from the batteries. Similarly, while recharging due to the regenerative braking, the proposed method removes the above-average peaks of the charging current of UCs. The proposed topology along with the EMS provides better state of charge (SoC) levels, giving a 38.6% increase in SoH levels of the batteries.

3.1 SoC estimation

The SoC estimation is very important and critical task to enhance the vehicle performance. The detailed of this research work has been discussed in the forthcoming sections.

3.1.1 Introduction

The battery management system is an integral part of any (variant of electric vehicle, X stands for B/H/PH) XEV. There are various batteries available in the market, but the lithium-ion batteries are gaining popularity [190]. They are equipped with several advantages such as high specific energy, low self-discharge rate, high energy density, prolong life, high charge/discharge and high cell potential, therefore, they have found a unique place in EV applications as ESS. Traction batteries need attributes like high energy density and power density. However, it is also associated with some demerits such as high cost, safety issues, ageing and immature technology. The selection of Li-ion batteries for traction application can be held true by comparing the energy density various batteries [191]–[194]. The batteries yield non-linear and complex characteristics making their behaviour unpredictable. The batteries undergo certain cycles with consideration of environmental condition, therefore battery circuit modelling is a prominent task in determining the accurate state of charge (SoC) and its performances. The model validation using parameter optimization is an essential tool to accurately predict the behaviour.

3.1.1.1. Literature review on the SoC estimation methods

There are various papers reported in the literature citing different SoC estimation methods. Some recent papers have been presented in this section.

The SoC basically is the measure of the remaining capability of the battery. The various methods which have been proposed to estimate the SoC can be categorized as: simple calculation methods, information-driven strategies, and model-based methods. The simple calculation method can further be divided into impedance, open-circuit voltage (OCV) and ampere-hour counting methods. The information-driven strategies are alike simple calculation methods except they use intelligent (neural networks, fuzzy logic, etc.) algorithms to train the model. Model-based methods consider battery as a dynamic system and involve state space to carry out battery modelling. This also uses observers like extended Kalman filter (EKF) and unscented Kalman filter (UKF) to estimate the state. Model-based techniques have some merits like high accuracy, fast convergence, and a good computing power [194]–[202]. In [204], the author has used the neural network (NN) for

estimation of SoC. Here, OCV was divided into three parts based on charging, discharging, and neutral mode and were fed to NN for correct estimation of SoC.

In [205], the reuse of EV batteries in the applications other than transportation has been suggested. The flow management of energy has also been explained. The author in [206] has discussed the role of the dual EKF (DEKF) for battery SoC and SoH estimation. Based on the comparison of simulation results using KF and DEKF, they recommended DEKF. In [207], a new method of combining DEKF algorithm and charging voltage curve for SoC estimation has been proposed. In [208], the adaptive SoC estimator has been proposed under various assumption and condition. The error estimate in SoC is less than 3% for both the constant current-voltage charging conditions and the dynamic discharging conditions. In,[209], the SoC and state-of-energy (SoE) are evaluated by the particles filter method and EKF by minimizing the errors in voltage or current signal measurement. The [210] addresses the estimation of battery SoC from the joint perspectives of dynamic data-driven and model-based recursive analysis.

In [211], the battery degradation capacity and the corresponding SoC has been estimated by using three-dimensional response surface-based battery OCV. In [212], a SoH estimation method has been proposed for lithium-ion batteries. Here, OCV and Thevenin's equivalent circuit model was used to improve the model accuracy and also to discuss the relation between internal parameters and states of the battery. In [213], a new kind of battery model which gets turned on/off based on the load response has been proposed. The various switching algorithm for the load has also been designed as well. The SoC and online model parameters co-estimation for liquid metal batteries has been proposed in [214]. In [215], SoC estimation of battery has been carried by applying two proportional-integral (PI) filters to minimize the sate error. In [216] a comparative study of ANN/KF for on-board SOC estimation has been carried out. They concluded that UKF presents the best overall performance. In [217] the SoC estimation with accuracy has been proposed. An attempt to estimate the OCV and SoC of the battery during normal operation of EV was made by means of charge/discharge current and voltage in [218].

From the above literature, it has been concluded that the major challenges which make battery inefficient are as follows: cell unbalancing, battery modelling, life of a battery, the effect of temperature, self-discharge, rate of charge and discharge, challenges of monitoring battery health, estimation of maximum capacity and communication method.

Out of these challenges, the battery modelling and temperature effect has been taken into consideration in our work and for cell balancing it has been assumed that the cell equalizer has been incorporated with BMS which will uniformly distribute the SoC of an individual cell.

3.1.1.2. Fixing the number of time constants (RC branches)

It has also been observed that many of the researchers have used different combination of RC circuits in battery modelling. To accurately estimate the SoC, the fixing of RC circuits in battery model is a must and the same is explained below.

In Fig. 3.1.1, five different time constant combinations have been considered. The OCV is compared for these five combinations (1/2/3/4/5 RC pairs respectively) and for a realistic battery. The zoom-in a portion of the waveform has been shown on the right side so that the clear waveform of all five times constants can be seen. In Fig. 3.1.1, it can be clearly seen that out of five combinations, the one with single RC pair is not at all acceptable. Out of remaining combinations, the blue dotted line (3-RC pair) is in close resemblance with the data of the OCV (green line). This also provides a minimal error in SoC estimation with realistic data. Therefore 3- RC combination is chosen here which is less explored in the literature.

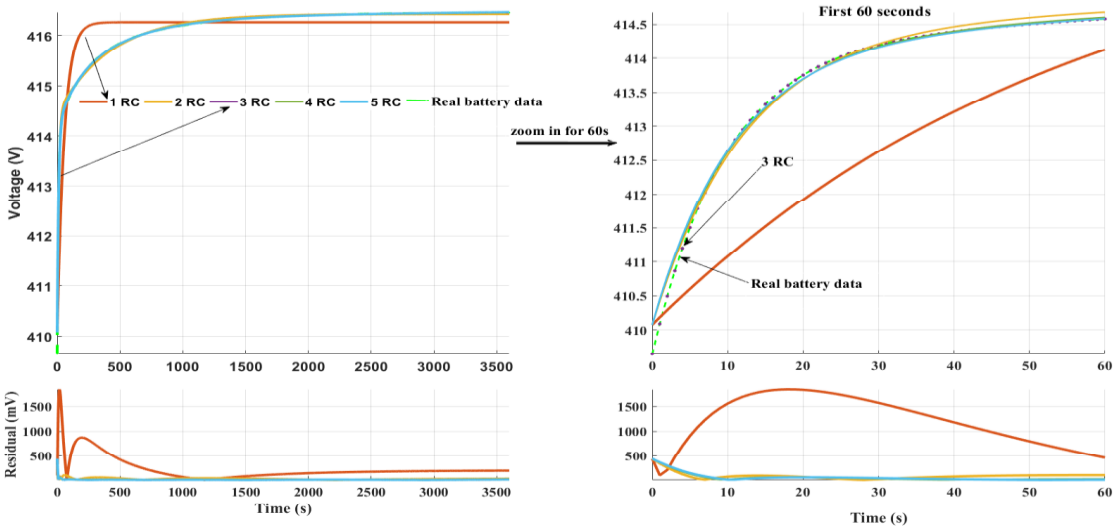

Fig. 3.1.1 Time constant comparison by curve fitting method

3.1.2. Equivalent circuit model

In this study, a Li-ion battery model is established. A reliable and accurate battery model is required to estimate battery SoC while using the model-based method. The third-order RC model of battery is crafted here in order to imitate the behavior of the real battery. The

model considered in this work consists of DC source, R_0, i.e. internal resistance and 3-parallel RC circuit in series as shown in Fig. 3.1.2.

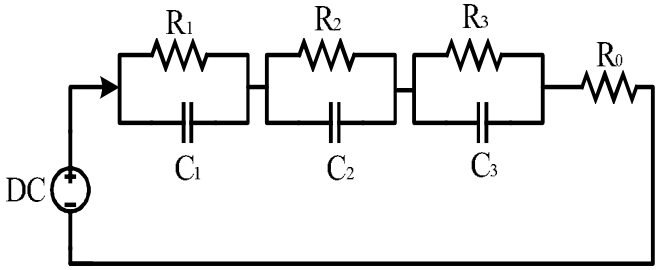

Fig. 3.1.2 The equivalent circuit battery model.

In a Li-ion battery, Li-ions move from anode to cathode through an organic electrolyte during discharging. During charging the reverse process is followed. Anode and cathode have a layered structure and Li-ions move in between layers. The governing chemical reactions are as follows:

$$\text{At cathode}: Li_{1-x}CoO_2 + xLi^+ + xe^- \rightarrow LiCoO_2$$
$$\text{At anode}: \quad Li_xC_6 \rightarrow xLi^+ + xe^- + 6C$$

The specification of the battery used has been shown in Table 3.1.1.

Table 3.1.1 Specification of the Li-ion battery [219], [220]

Commercialization year	1992
Cell voltage	3.7
Energy by weight (Wh/kg)	90-180
Specific power (W/kg)	760
Energy by volume (Wh/L)	220 –350
Maximum discharge rate	40C
Recharge time	< 3 Hours
Cycle life cycle	1200
Self-discharge per month	5% - 10%
Temperature range ^{0}C	-20°C to + 60°C-
Preferred charge method	Constant voltage and constant current
Average energy cost	$250/kWh

3.1.3. Identification of battery model parameter

The battery performance depends on three main parameters, i.e. SoC, operating temperature, and ageing. The battery model parameter identification is obtained by the discharging/charging current pulse experiments, and the specific experimental steps are described as follows:

1. Rest the single battery for more than 24 hours, to ensure that the polarization voltage of the battery is reduced to zero.
2. Discharge the single battery with a constant current.
3. Rest the battery at the end of the experiment.

From Fig. 3.3, it is clear that the response voltage has a downward jump to discharge the battery once the battery is at rest for long enough. Similarly, the response voltage has an upward jump for charging the battery. The voltage drop due to R_o is sudden, whereas it is gradual for the RC combination.

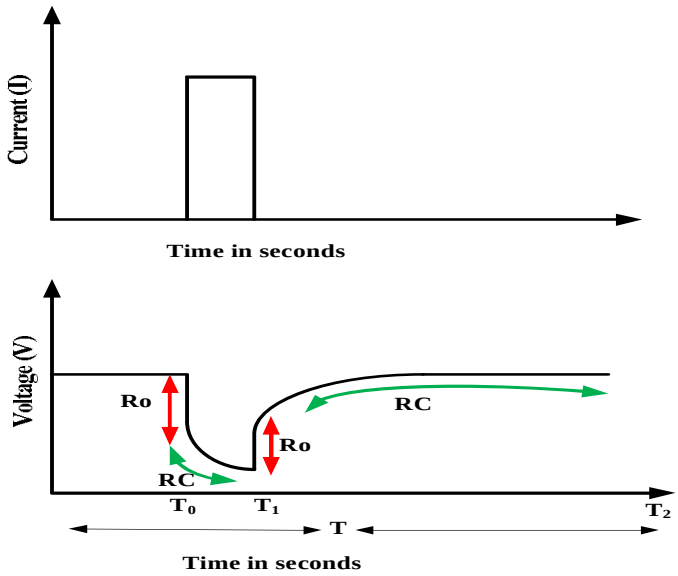

Fig. 3.1.3 Discharge test at constant current pulse

According to the principle of the circuit, the calculation of ohmic resistance could be obtained by the formula.

$$V_{ter} = V_{OC} - V_0 - V_1 - V_2 - V_3 \tag{3.1.1}$$

Where V_{ter} is the terminal voltage, V_{oc} open-circuit voltage, V_o is the voltage across the resistance R_o, V_1 voltage across resistance R_1, V_2 voltage across resistance R_2 and V_3 voltage across resistance R_3

$$V_0 = IR_0 \tag{3.1.2}$$

$$C_1 \frac{dV_1}{dt} + \frac{V_1}{R_1} = I \tag{3.1.3}$$

$$C_2 \frac{dV_2}{dt} + \frac{V_2}{R_2} = I \tag{3.1.4}$$

$$C_3 \frac{dV_3}{dt} + \frac{V_3}{R_3} = I \tag{3.1.5}$$

The time constant of the circuit can be expressed as

$$\left.\begin{aligned} \tau_1 &= R_1 C_1 \\ \tau_2 &= R_2 C_2 \\ \tau_3 &= R_3 C_3 \end{aligned}\right\} \tag{3.1.6}$$

Determination of V_{oc}: Since the battery has been at rest for sufficiently long time and the test starts from zero state, we have:

$$V_{OC} = V_{ter}(T_0^-) \tag{3.1.7}$$

The R_0 can be obtained by

$$R_0 = \frac{V_{ter}(T_0^-) - V_{ter}(T_0^+)}{I} \tag{3.1.8}$$

Where T_0^- and T_0^+ represent the initial conditions

The time duration from the T_0^+ to T_2 has been used to calculate the three-time constants. During this period the circuit is in zero input response

$$\left.\begin{aligned} V_{1zero} &= V_1(T_1) \\ V_{2zero} &= V_2(T_1) \\ V_{3zero} &= V_3(T_1) \end{aligned}\right\} \tag{3.1.9}$$

From Eq (3.1.3), (3.1.4) and (3.1.5)

$$\left.\begin{aligned} V_1(T - T_1) &= V_{1zero} e^{\frac{T-T_1}{\tau_1}} \\ V_2(T - T_1) &= V_{2zero} e^{\frac{T-T_1}{\tau_2}} \\ V_3(T - T_1) &= V_{3zero} e^{\frac{T-T_1}{\tau_3}} \end{aligned}\right\} \tag{3.1.10}$$

Since I = 0, from (3.1.1) and (3.1.2)

$$V_{ter} = V_{oc} - V_1(T - T_1) - V_2(T - T_1) - V_3(T - T_1) \tag{3.1.11}$$

Considering $H = V_1 + V_2 + V_3$

This yields

$$H(T - T_1) = V_{1zero} e^{\frac{T-T_1}{\tau_1}} + V_{2zero} e^{\frac{T-T_1}{\tau_2}} + V_{3zero} e^{\frac{T-T_1}{\tau_3}} \tag{3.1.12}$$

From Eq (3.1.10)

$$H(T-T_1)=V_{oc}-V_{ter}(T-T_1) \tag{3.1.13}$$

To establish a regression equation that can be used for parameter identification, the following two variables are taken from [221].

$$X(T-T_1)=\int_{T_1}^{T}H(\tau-T_1)d\tau \tag{3.1.14}$$

$$Y(T-T_1)=\int_{T_1}^{T}X(\tau-T_1)d\tau \tag{3.1.15}$$

$$X(T-T_1)=(V_{1zero}\tau_1+V_{2zero}\tau_2+V_{3zero}\tau_3)-(V_{1zero}e^{\frac{T-T_1}{\tau_1}}+V_{2zero}e^{\frac{T-T_1}{\tau_2}}+V_{3zero}e^{\frac{T-T_1}{\tau_3}}) \tag{3.1.16}$$

$$Y(T-T_1)=(V_{1zero}\tau_1+V_{2zero}\tau_2+V_{3zero}\tau_3)(T-T_1)-(V_{1zero}\tau_1^2+V_{2zero}\tau_2^2+V_{3zero}\tau_3^2)+(V_{1zero}\tau_1^2e^{\frac{T-T_1}{\tau_1}}+V_{2zero}\tau_2^2e^{\frac{T-T_1}{\tau_2}}+V_{3zero}\tau_3^2e^{\frac{T-T_1}{\tau_3}}) \tag{3.1.17}$$

By using Eq. (3.1.13), (3.1.16) and (3.1.17)

$$Y(T-T_1)=-X(T-T_1)(\tau_1+\tau_2+\tau_3)-H(T-T_1)\tau_1\tau_2\tau_3+(V_{1zero}\tau_1+V_{2zero}\tau_2+V_{3zero}\tau_3)(T-T_1)+(V_{1zero}+V_{2zero}+V_{3zero})\tau_1\tau_2\tau_3 \tag{3.1.18}$$

When these expressions are substituted into the third equation, a regression equation is obtained as follows, which has no exponential terms in it:

$$Y(T-T_1)=[-X(T-T_1)\quad -H(T-T_1)\quad (T-T_1)\quad 1]\begin{bmatrix}\tau_1+\tau_2+\tau_3\\ \tau_1\tau_2\tau_3\\ V_{1zero}\tau_1+V_{2zero}\tau_2+V_{3zero}\tau_3\\ (V_{1zero}+V_{2zero}+V_{3zero})\tau_1\tau_2\tau_3\end{bmatrix} \tag{3.1.19}$$

The time constants and initial states V_{1zero}, V_{2zero} and V_{3zero} can be calculated by Eq (3.1.19) by considering all the sampling point from T_1^+ to T_2

Then from Eq. (3.1.19) we have

$$\begin{bmatrix}Y_1\\ Y_2\\ \dots.\\ Y_n\end{bmatrix}=\begin{bmatrix}-X_1 & -H_1 & T-T_1 & 1\\ -X_2 & -H_2 & T_2-T_1 & 1\\ \dots.. & \dots.. & \dots.. & \dots.\\ -X_2 & -H_n & T_n-T_1 & 1\end{bmatrix}\begin{bmatrix}\tau_1+\tau_2+\tau_3\\ \tau_1\tau_2\tau_3\\ V_{1zero}\tau_1+V_{2zero}\tau_2+V_{3zero}\tau_3\\ (V_{1zero}+V_{2zero}+V_{3zero})\tau_1\tau_2\tau_3\end{bmatrix} \tag{3.1.20}$$

$$B=\begin{bmatrix} Y_1 \\ Y_2 \\ .... \\ Y_n \end{bmatrix} A=\begin{bmatrix} -X_1 & -H_1 & T-T_1 & 1 \\ -X_2 & -H_2 & T_2-T_1 & 1 \\ ..... & ..... & ..... & .... \\ -X_2 & -H_n & T_n-T_1 & 1 \end{bmatrix} P=\begin{bmatrix} \tau_1+\tau_2+\tau_3 \\ \tau_1\tau_2\tau_3 \\ V_{1zero}\tau_1+V_{2zero}\tau_2+V_{3zero}\tau_3 \\ (V_{1zero}+V_{2zero}+V_{3zero})\tau_1\tau_2\tau_3 \end{bmatrix} \quad (3.1.21)$$

The Eq. (3.1.20) can be written as

$$B=AP \quad (3.1.22)$$

By least squared error solution

$$P=(A^TA)A^TB \quad (3.1.23)$$

$$\left.\begin{aligned} V_{1zero}&=IR_1(1-e^{\frac{T_1}{\tau_1}}) \\ V_{2zero}&=IR_1(1-e^{\frac{T_1}{\tau_2}}) \\ V_{3zero}&=IR_1(1-e^{\frac{T_1}{\tau_3}}) \end{aligned}\right\} \quad (3.1.24)$$

Since V_{1zero} and V_{2zero} are already obtained, R_1 and R_2 can be calculated from (3.1.24) and subsequently, C_1 and C_2 can be calculated from (3.1.6).

3.1.3.1 *State of charge estimation:*

The output voltage can be calculated as [222]

$$V_{ter}=V_{oc}(t)-i(t)\left[R_0-\left\{\left(\frac{R_1+2R_0}{R_1C_1}\right)e^{-\left(\frac{t}{\tau_1}\right)}\right\}-\left\{\left(\frac{R_2+2R_0}{R_2C_2}\right)e^{-\left(\frac{t}{\tau_2}\right)}\right\}-\left\{\left(\frac{R_3+2R_0}{R_3C_3}\right)e^{-\left(\frac{t}{\tau_3}\right)}\right\}\right] \quad (3.1.25)$$

A) *SoC_V Calculation:* Cell voltage when all the reactions are balanced, is called equilibrium voltage, which is occasionally referred to as OCV. With this OCV, voltages based SoC (SoC_v) can be estimated using [223]–[226]

$$SoC_v=\frac{1}{a_1}(OCV-a_0) \quad (3.1.26)$$

Where a_0 is battery terminal voltage when SoC = 0% and a_1 is battery terminal voltage when SoC = 100%. But, due to change in temperature, equilibrium voltage of the battery at any temperature (T_{em}) gets changed as

$$V(T_{em})=V_{298}+(\frac{dV}{dT_{em}})(T_{em}-298) \quad (3.1.27)$$

$\frac{dV}{dT_{em}}$ is temperature coefficient and is constant for the considered temperature range. So the consideration of this OCV with temperature effect will lead to modifying SoC_V and will contribute in the final SoC calculation.

B) *SoC Calculation:* The coulomb counting (CC) method involves the current integration flowing through the battery to get SoC

$$SoC_i = \frac{1}{c_p}\left(c_p - \int Idt\right) \tag{3.1.28}$$

C_p is battery capacity in Ah. Due to change in temperature, the cell reaction rate gets changed. The Arrhenius equation, the reaction rate is given as

$$K = K_0 \times e^{\left(\frac{-E_a}{R \times Tem}\right)} \tag{3.1.29}$$

K_0 is reaction constant, R is gas constant, E_a is activation energy, and Tem is operating temperature. During the electron transfer reaction, electrons require the additional amount of energy to surmount the energy barrier called the activation energy (E_a= J·mol^{-1}) which depends on temperature. As for every 10 ^oC temperature increase, the current gets doubled so for ΔT_{em} temperature change, final equation can be written as.

$$I_{(s-d)} = \frac{1}{c_p} K_O(T_{em}) e^{-\left(\ln 2(\frac{R}{10})\right)(T_{em} \times (T_{em}+10))} \tag{3.1.30}$$

Temperature effect and self-discharge current are included for analyzing run-time characteristics. A number of Li-ion cells are connected in series and in parallel to simulate a powerful battery to be used in hybrid vehicles. The output voltage is calculated as Eq. (3.1.25) where V(t) is time-dependent OCV, i(t) is the time-dependent current, and multiplier term associated with i(t) represents the impedance offered. From Eq. (3.1.26), temperature-dependent voltage-based SoC, that is, $SoC_V(T_{em})$, can be calculated as Eq. (3.1.31) and from Eq. (3.1.28) temperature-dependent current based SoC, that is, SoC_i(Tem), can be calculated as Eq. (3.1.32)

$$SoC_v(T_{em}) = \frac{1}{a_1}\left[\left\{V_{ter}(t) + \left(i(t) \times 2^{\left(\frac{\Delta T_{em}}{10}\right)} + I_{(s-d)}(t)\right) \times R_0 - \left\{\left(\frac{R_1 + 2R_0}{R_1 C_1}\right) e^{-\left(\frac{t}{\tau_1}\right)}\right\} - \left\{\left(\frac{R_2 + 2R_0}{R_2 C_2}\right) e^{-\left(\frac{t}{\tau_2}\right)}\right\} - \left\{\left(\frac{R_3 + 2R_0}{R_3 C_3}\right) e^{-\left(\frac{t}{\tau_3}\right)}\right\}\right\} + \left(\frac{dV}{dT_{em}}\right)(T_{em} - 298) - a_0\right] \tag{3.1.31}$$

$$SoC_i(T_{em}) = \frac{1}{c_p}\left[c_p - \int \left\{i(t) \times 2^{\left(\frac{\Delta T_{em}}{10}\right)} + I_{(s-d)}(t)\right\} dt\right] \tag{3.1.32}$$

3.1.3.2. Simulations Results and Discussion:

The SoC indicates the power available in a battery and its correct information is of utmost importance. The parameters namely resistance and capacitance, play a vital role in system dynamic performance so to accurately estimate the SoC, these parameters are first optimized.

The procedure of parameter estimation starts with the data collection of the battery, which involves OCV and charge/discharge current pulse data collection. The collected data is processed to identify the effects of R_o and the RC pairs on OCV while tracking the charge/discharge current pulse. The OCV is sampled so that its magnitude can be located at various time intervals concerning the current pulse. Then parameters are mathematically estimated by the Eq. (3.1.1) to Eq. (3.1.24). The obtained parameters are again optimized with the help of a function called "lsqnonlin" provided in the MATLAB. The obtained parameters are put up in the battery block, and an accurate SoC can be obtained. The obtained SoC with the 3-RC circuit is compared with the original circuit (circuit having no change). The procedure of the parameter estimation of the 3-RC circuit has been shown in Fig. 3.1.4 in the form of a flowchart.

The simulation has been carried out in MATLAB/Simulink, and the temperature has been kept 303° K to 315° K for the whole experiment. The data of a real battery has been collected and is fed in the MATLAB with the help of a lookup table [227]. After that the OCV and current discharge pulse have been tracked with the SoC at the same time. The pairs due to R_o and RC also need to be identified for a sampling of the data, as shown in Fig. 3.1.5:

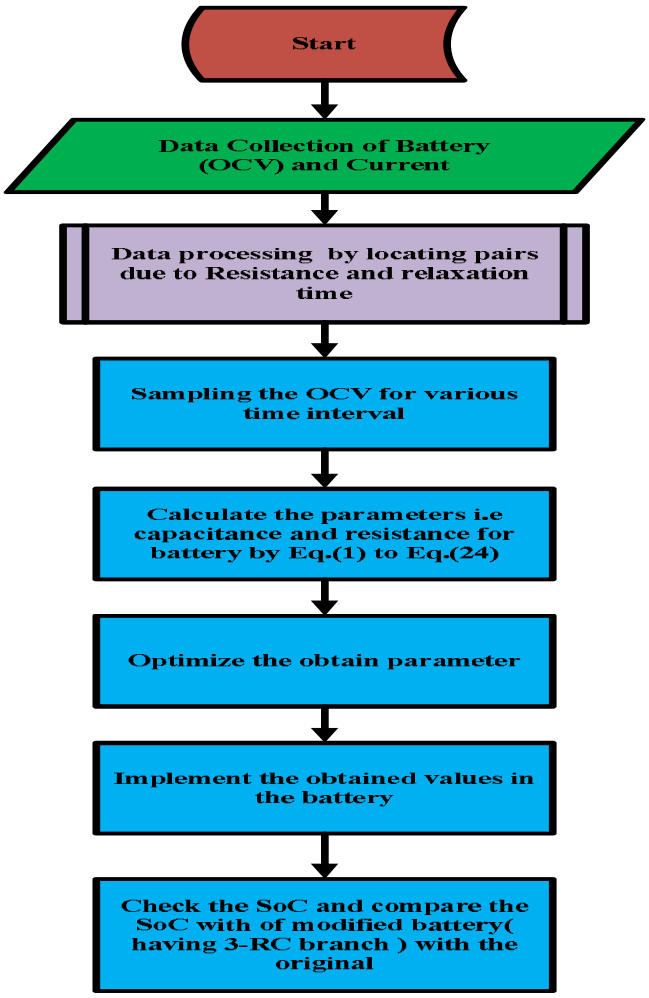

Fig. 3.1.4 Flow chart of estimation of parameters

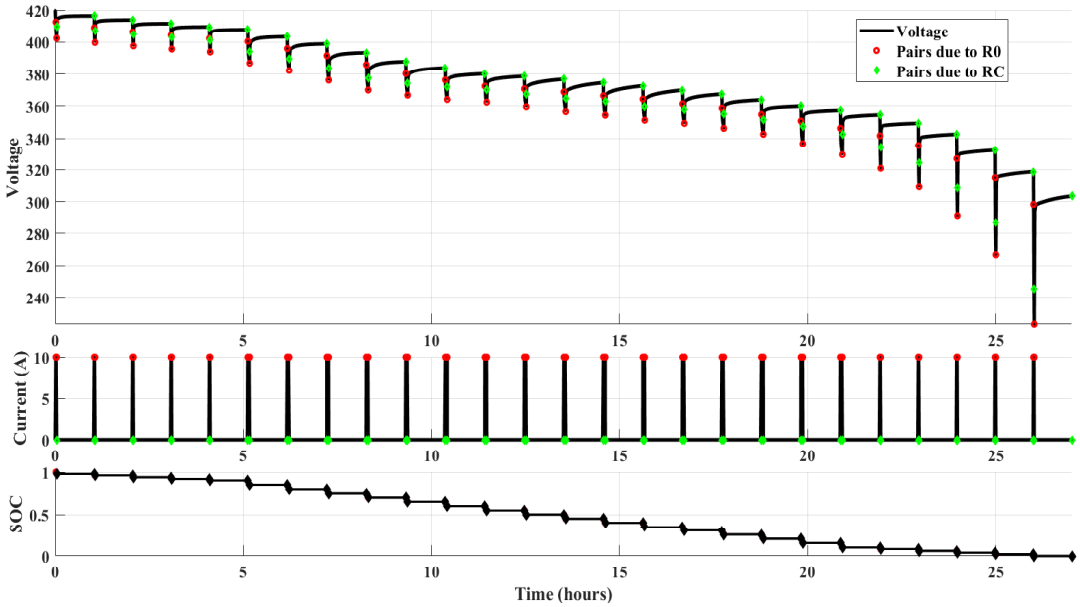

Fig. 3.1.5 The data of the battery and the located pairs due to R_0 and RC

The difference in the behaviour of the real data of a battery and the simulated battery, which has been demonstrated in Fig. 3.1.6:

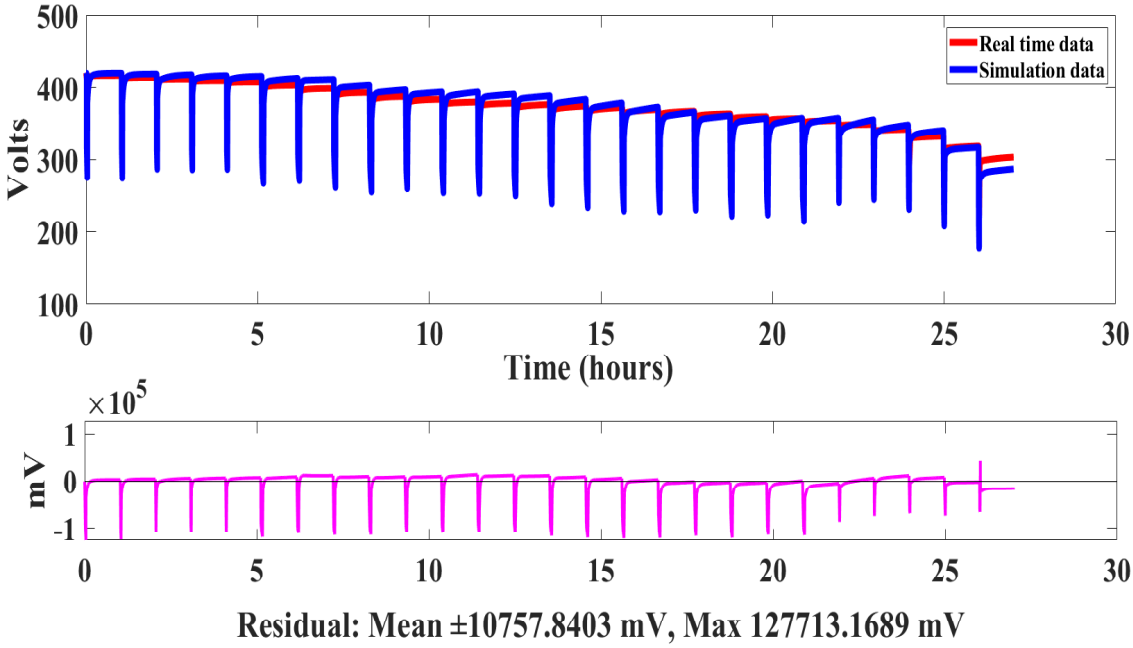

Fig. 3.1.6 The real-time data and simulated data of battery

By locating the pairs and by sampling the OCV and corresponding current pulse for the time interval T_0 to T_2, the parameters can be calculated using the equations described in section 3.1.3. The obtained parameters have been shown in Fig. 3.1.7. The time constant and resistance are calculated by applying the equations mentioned in section 2 and are given below.

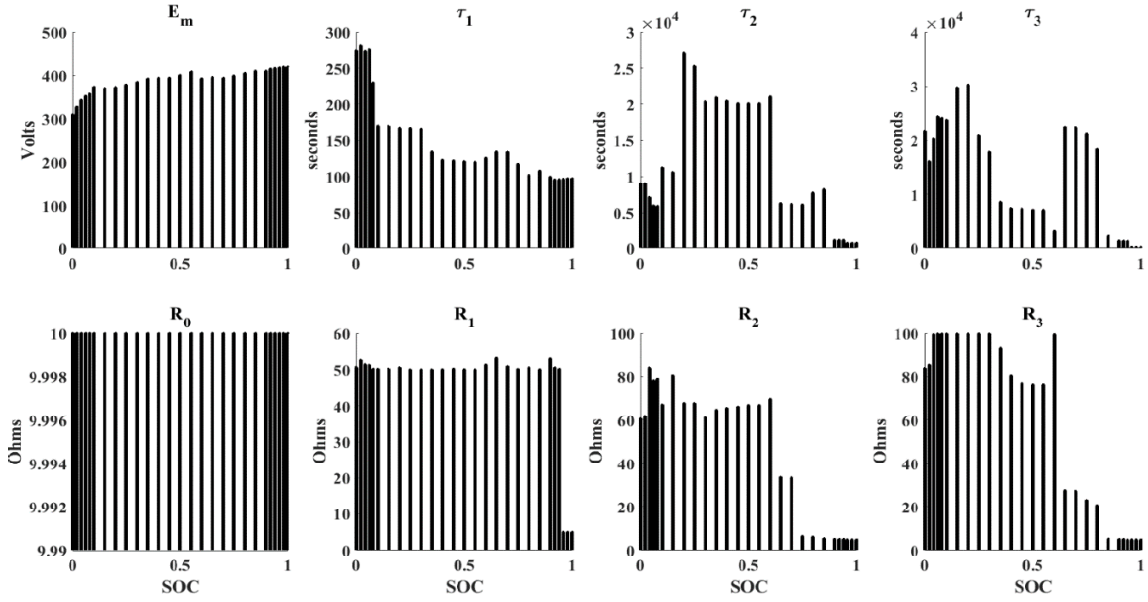

Fig. 3.1.7 The parameter obtained for the 3-RC circuit

The obtained parameters have been optimized utilizing "lsqnonlin" function provided in MATLAB. The logic of using the lsqnonlin function is that this function is very useful for solving the nonlinear least squares problems. It has some more advantages like:

- One only needs to specify the function, no Jacobian needed.
- It works better than Gauss-Newton if the solution is far away.
- There are many options available: one can specify Step Tolerance, Function Tolerance,
- It also displays information after each iteration.

The values of the parameters have been provided using the graphs shown below in Fig. 3.8.

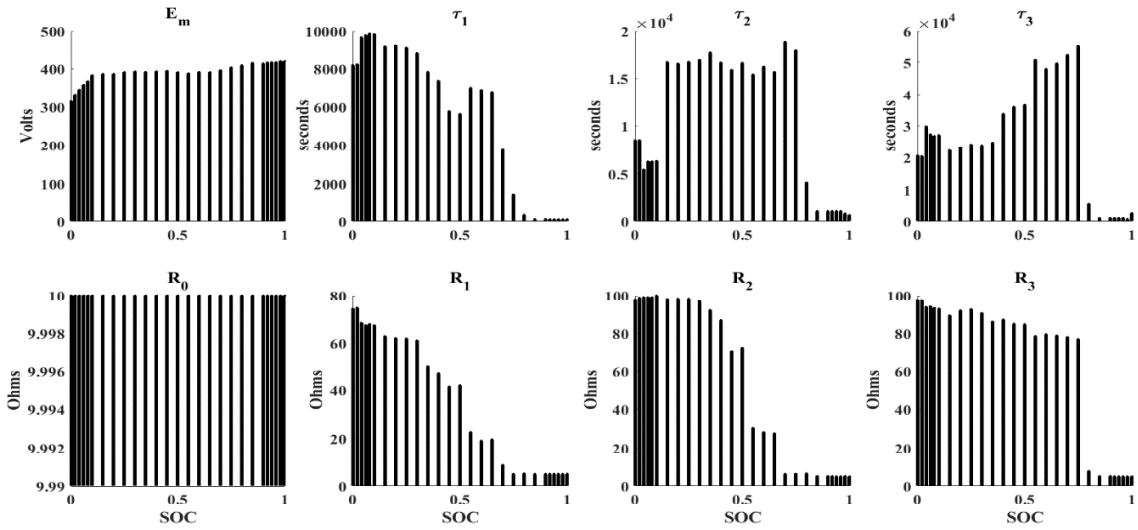

Fig. 3.1.8 The optimized parameter obtained for the 3-RC circuit

The obtained parameters have been fed to the modified block of 3-RC pair circuit and are compared with the SoC of the original circuit, as shown in Fig. 3.1.9 below. In the Fig. 3.1.9 the new SoC is the SoC obtained by modifying the battery model by incorporating 3-RC branches and original SoC is the SoC of the battery without any modification or for default battery model. The curves show the real value curve of SoC estimation. The coulomb-counting and OCV methods have been used to estimate the SoC.

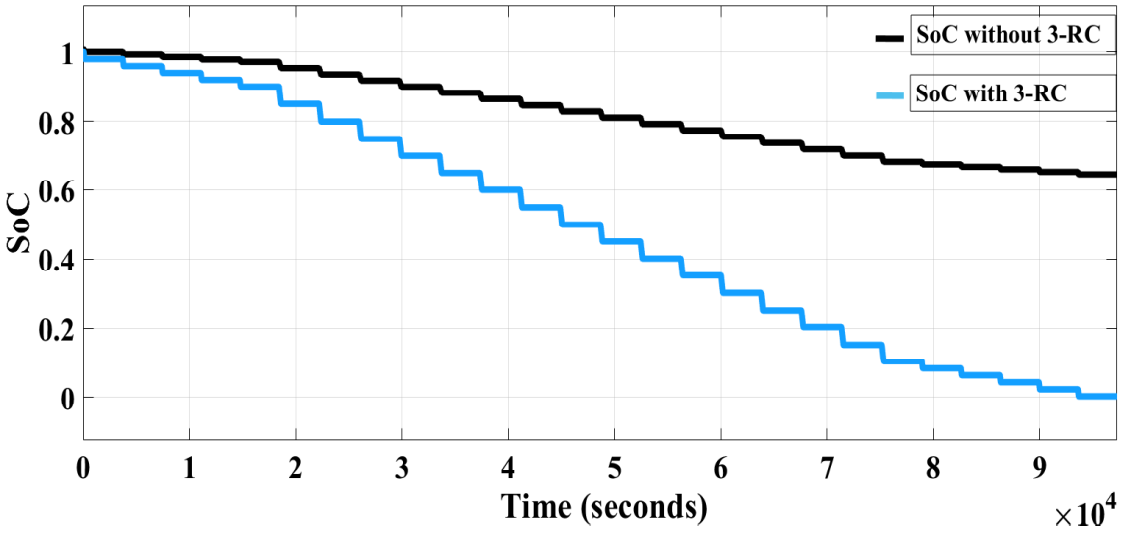

Fig. 3.1.9 The new and original SoC comparison and their variation with respect to time

3.1.4. The ANFIS based Optimized SoC

The obtained parameters have been installed in the circuit shown in Fig.3.1.10 and are used to obtain the new SoC. The obtained SoC has again been optimized by ANFIS, as shown below:

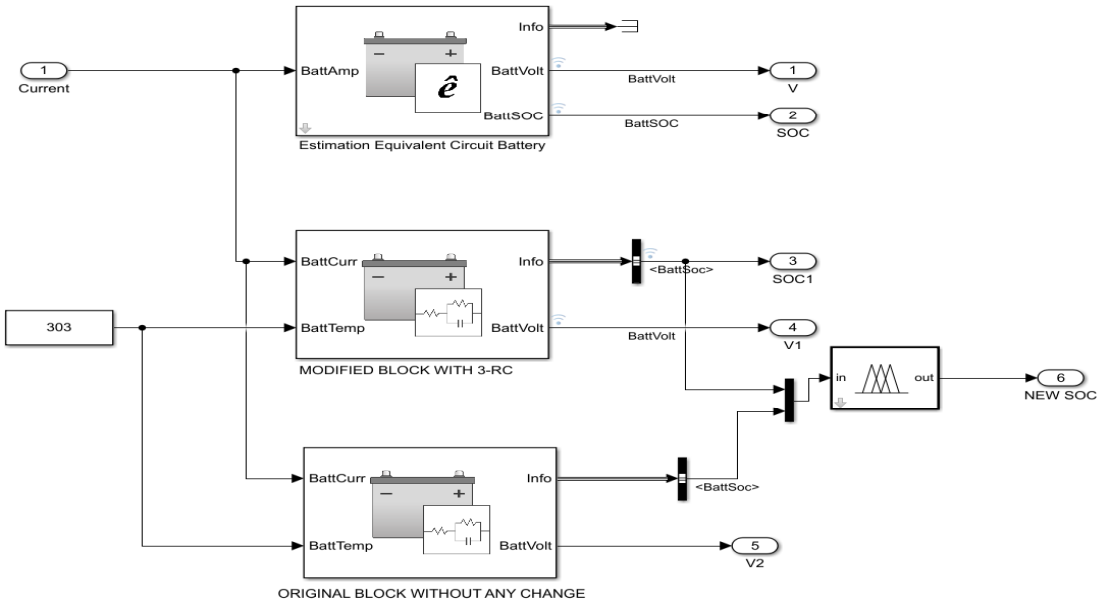

Fig. 3.1.10 The MATLAB/Simulink circuit used to simulate and analyze SoC

***ANFIS algorithm*:** The ANFIS has many advantages like it does not necessitate the use whole mathematical model only input-output data are required generated from the simulation. The rousing features of the NN are its ability to learn and adapt, whereas the ability of a fuzzy system is to consider imprecision and prevailing uncertainties. In order to exploit the advantages of both methods, an adaptive neuro-fuzzy inference system

(ANFIS) algorithm comprising of both the NN and the fuzzy logic is adapted for the proposed work. The ANFIS do have a high computational cost but due to the redundancy, complementarity, heterogeneity and its performance make it a fascinating tool for such case. As the learning rate of the NN is relatively low, which makes it less suitable as a stand-alone technique for time-critical applications, integrating it with fuzzy logic brings a better real-time response.

The EV applications deals with high uncertainty of the power demand, temperature, and load variations. Concurrently, the system should also be designed in such away so that it could be adaptive and responsive to these changes. Therefore, application of ANFIS is appropriate for the proposed system. Further, the literature survey establishes that ANFIS results in accurate modelling of the system provided a good data bank is available. This is the icing on the cake for the system under consideration, as the authors can generate the data set. As expected, the ANFIS optimized SoC provides lesser variation in parameters during dynamically load change and lesser settling time. The real-time verification ensures that this can be implemented practically. ANFIS is a hybrid of ANN and FLC, which enjoys the benefits of both. A dynamic and parallel processing system estimates input-output functions. A fuzzy method adaptively deduces and alters its fuzzy relationship from representative mathematical samples. The NN, on the other hand, can erratically create and refine fuzzy rules from the training data. The fuzzy sets are thought to be constructive in the intelligent field and in dealing with higher processing. The performance of FLC depends on the rule basis, number, and forms of membership functions (MFs). In this work, various MFs like triangular, trapezoidal, and Gaussian are evaluated. Out of these, triangular is chosen here as it offers minimum error and less computational burden. The authors have tested the system with fuzzy MF rules like 3*3, 5*5, and 7*7, but they all yield the same result and settling time. Therefore, 3*3 rules are chosen here because of the lesser computational burden. The fuzzy input, along with triangular MF, is fed into the NN block. The NN block consists of a rule base, which is connected to the fuzzy inference system (FIS). Here, back propagation (BP) algorithm issued to train the FIS, and the BP learning algorithm has been used for training feedforward NNs. The most commonly used FIS are Mamdani and Sugeno. In this work, the Sugeno-type FIS is used because it is computationally efficient than the Mamdani type and can be trained by real data as opposed to the latter, which is more susceptible on an expert system. Also, the output MF of the

Sugeno system is either linear or constant. Takagi Sugeno FIS is executed here using ANFIS and has a five-layered structure, as shown in Fig. 3.1.11.

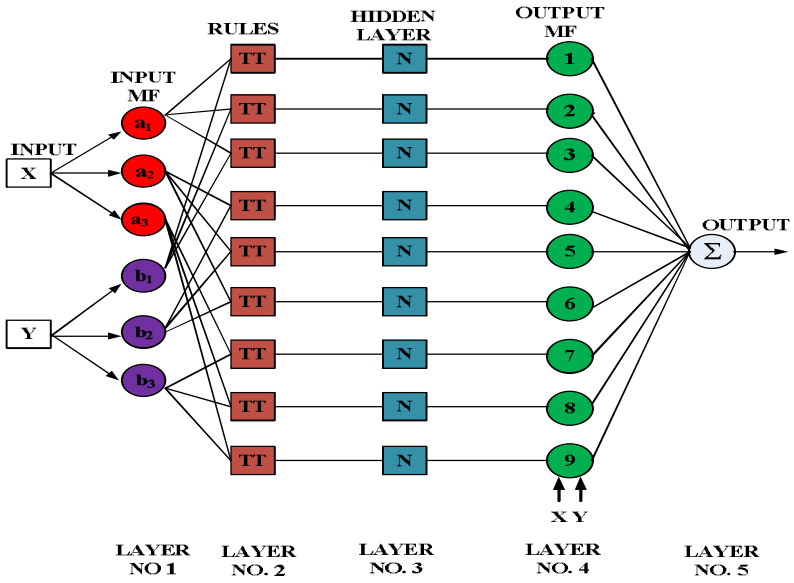

Fig. 3.1.11 Structure of ANFIS

Fuzzification of the input variable has been done in the first hidden layer and T-standard operators to compute the rule are conveyed to the second hidden layer. Third and fourth hidden layers standardize the rule strengths and determine consequent parameters of the rule, respectively. The fifth layer computes the overall input by summing all the incoming signals. ANFIS architecture is an adaptive, feedforward network structure. Every node plays out a specific function on input signals as well as on the set of parameters of that node. Some of the nodes are adaptive, which means that the node parameters are dependent on the other nodes; whereas others are fixed nodes, where the node parameters are independent.

The MF chosen should be able to minimize the error between the actual output data and ANFIS input sketched output data. The parameters connected with the MF will change within the learning process.

Layer 1: This layer contains two inputs, one as error and other as a change in error represented by x and y respectively. It is commonly known as the fuzzification layer [228].

Layer 2: Every node of the 2^n (the number of fuzzy if-then rules) is fixed and labelled as Π. It multiplies the input signal and forwards and outputs the product as given by Eq. 3.1.33

$$p_k = \eta_{ai}(x) \times \eta_{bi}(y) \tag{3.1.33}$$

Where k = 1, 2, 3... 9. The output of each node represents the firing strength $\overline{p_i}$ (i= 1 to 2^n) of the *i* the fuzzy if-then rule given by Eq. 3.1.34 as

$$\overline{p_i} = \frac{p_i}{\sum_{i=1}^{2n} p_i} \tag{3.1.34}$$

Layer 3: Each node in this layered circle calculates the ratio of the individual rule's firing strength to the sum of all rules given by Eq. 3.1.35.

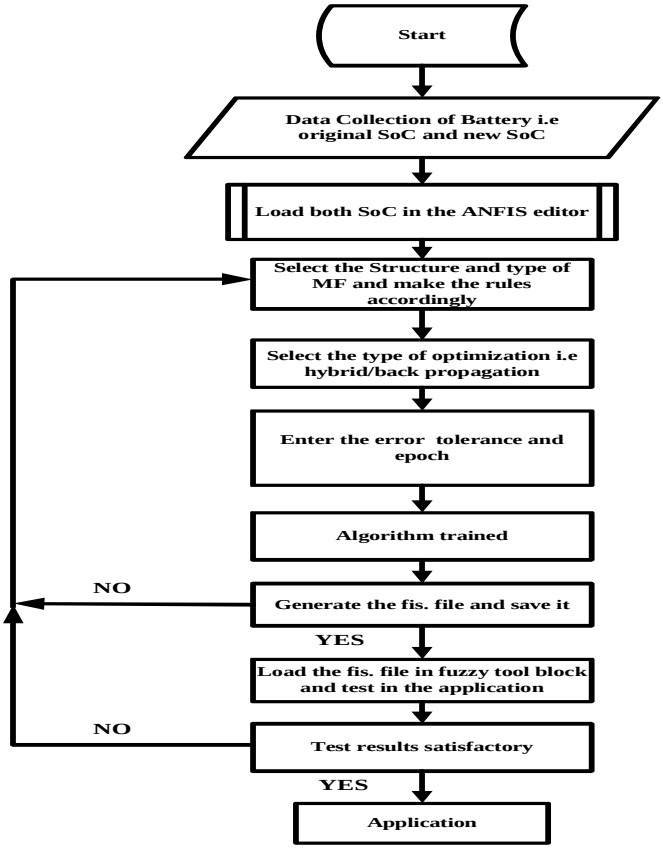

Fig. 3.1.12 Flowchart showing the operation of an adaptive neuro-fuzzy inference system (ANFIS) algorithm.

The ANFIS model for the controller design uses the architecture of the adaptive network. Fig. 3.1.12 shows the flow chart for the working operation of the ANFIS algorithm. The ANFIS model is designed, trained, and analyzed using MATLAB 2017b Neuro-Fuzzy Designer tool-box and graphical user interface (GUI).

A data set is collected and stored in the MATLAB workspace to train the ANFIS. The ANFIS is tested with different MFs such as triangular, trapezoidal, and Gauss MFs, and it is found that the training error is minimum with triangular MF. The epochs (iterations) and error are shown in Fig. 3.1.13.

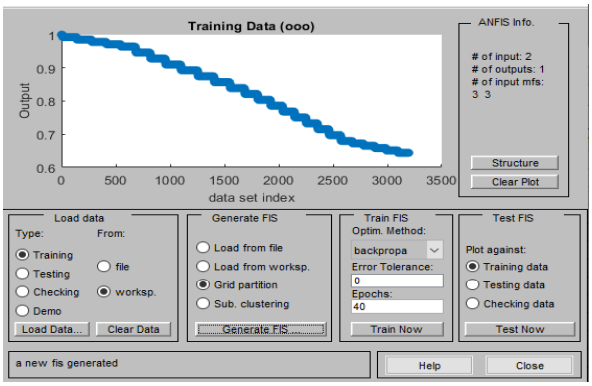

A) Training data

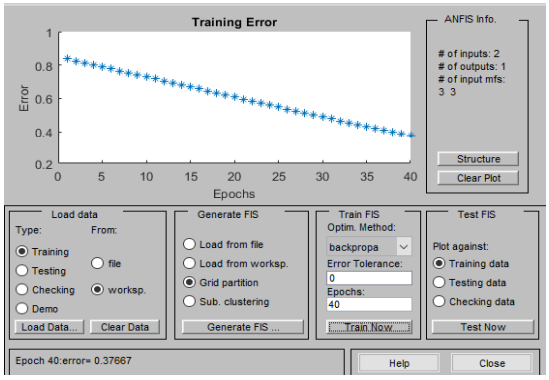

B), Epochs and test data error

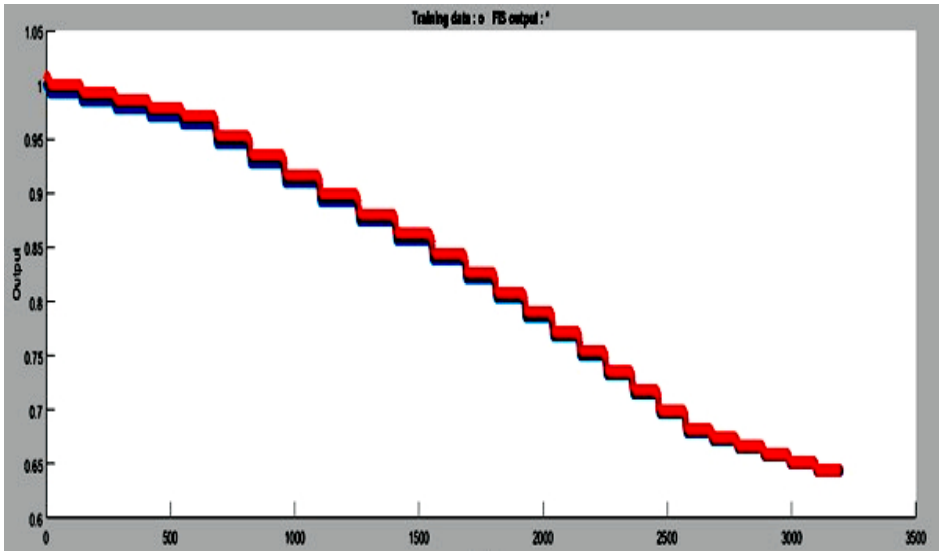

C) Training data testing

Fig. 3.1.13. A) Training data, B) Epochs and test data error, and C) Training data testing. The predicted output is indicated by red, and the test data is represented by blue circles.

$$\sigma^3 = \overline{p_i} = \frac{p_i}{p_1 + p_2}, i = 1,2,3. \tag{3.1.35}$$

Layer 4: This layer is called a defuzzification layer. It calculates the individual output values "f" from the inferring of the rule base. Each node in this layer is a square node, with the function as given by Eq 3.1.36

$$\sigma_i^4 = \overline{p_i} f_i = \overline{p_i}(g_i x + h_1 y + r_i), \tag{3.1.36}$$

Where i=1, 2, 3 and $\overline{p_i}$ is the output of layer 3 and $\{g_1, h_1, r_i\}$ is a parameter set. Parameters in this layer are also referred to as consequent parameters.

Layer 5: This layer is called as the output layer. There is a single circle of the output neuron labelled as Σ, and the output signal is obtained by adding up input signals as it can be seen in the following Eq 3.1.37.

$$\sigma_i^5 = \sum_i \overline{p_i} f_i = \frac{\sum ip_i f_i}{\Sigma} ip_i, \tag{3.1.37}$$

Comparison of simulated SoCs: Fig. 3.1.14 (A) provides the comparison of estimated SoCs, where red line indicates estimation without RC, and the blue line indicates with the 3-RC circuit. The circuit with 3-RC involves more losses due to the impedance whereas in another case losses due to internal resistance are only considered. The results obtained using RC pairs are closer to that of real data available in [38]. Therefore, the proposed approach provides a faster and accurate estimation of SoC in real-time. Fig. 3.1.14 (B) provides the OCV Vs SoC curve of the battery.

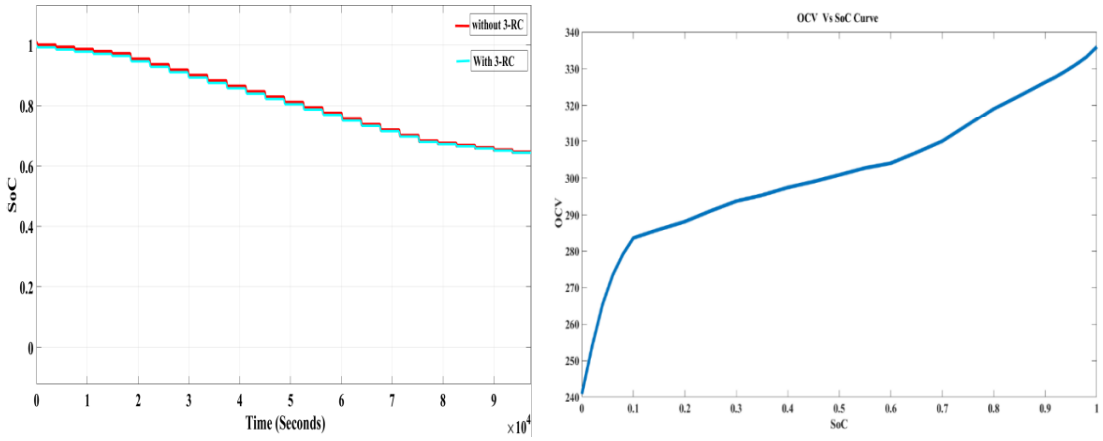

A) SoC comparison with 3-RC and ANFIS optimized & without 3-RC circuit

B) OCV versus SoC curve wih 3 RC

Fig. 3.1.14 A) SoC comparison with 3-RC and ANFIS optimized & without 3-RC circuit B) OCV versus SOC curve

This chapter presents the design of a data fusion algorithm based on ANFIS and provides minimal root mean square error and mean absolute percentage error. The redundancy, complementarity, timeliness, heterogeneity etc. are the advantages of the systems based on data fusion algorithms. As the learning rate of the NN is relatively low, which makes it less suitable as a stand-alone technique for time-critical applications, integrating it with fuzzy logic brings a better real-time response. The fuzzy logic creates a fuzzy engine based on the rules derived from the input/output data set. The neural network trains the engine for more precision. The steps of the algorithm have been presented below:

Algorithm

Step 1: Collect the data from individual sensors.

Step 2: Create a fuzzy engine with pre-determined input/output variables using ANFIS.

Step 3: Train/re-train the fuzzy engine until there is no improvement in the accuracy.

Step 4: Train the engine to obtain the minimum root mean square error.

Step 5: If No, go to step 4.

Step 6: If Yes, stop training further and save the ". fis" file.

Step 7: Implement the ".fis" in the fuzzy toolbox and obtain the results.

Step 8: Implement the same work in hardware to check its validity in real-time.

Step 9: The algorithm uses an ANFIS based system for fusing the data from multiple sources.

The two inputs are given to the ANFIS based algorithm by means of taking the Input/ Output data in the workspace of the MATAB tool. The generated ". mat" file is loaded in the ANFIS. The training has been carried by setting the epoch value and MF is generated using "trimf". The output which is ".fis" file is loaded in a fuzzy toolbox in the simulation model then the output is taken, and the same is checked in the HIL.

3.1.5. Variation of SoC and OCV with temperature

Two batteries, namely, A and B, have been taken with the 3-RC circuits. The behaviour of battery A has been captured for temperature variations from 40 ^{o}C to - 40 ^{o}C as shown in Fig. 3.1.15 below. The effect of temperatures is neglected in Battery. The current pulse of 2A has been considered for this purpose.

Simulation and analysis

At t = 0 s, the Battery A and B are discharged with 2 A at an ambient temperature of 40 °C.

At t = 150 s, the internal temperature has increased to its steady-state value of 42.2 °C due to heat losses from the discharge process. This causes the output voltage of Battery A to slightly increase, while battery B output voltage continues to decrease.

At t = 1000 s, the ambient temperature is decreased to -40 °C. This causes the output voltage of Battery A to greatly decrease as the internal temperature decreases rapidly. Also, the SoC of Battery A decreases due to the reduction of its capacity. The battery B output voltage continues to decrease slowly to its steady-state voltage.

At t = 2000 s, the ambient temperature is increased from -40 °C to 0 °C. As the internal temperature increases, the output voltage of Battery A increases. Also, as the capacity increases, the SoC of Battery A increases. The Battery B output voltage remains constant to its steady-state value.

At t = 2500 s, Battery A and B are charged with 3 A at an ambient temperature of 0 °C. This causes the internal temperature to increase due to heat losses during the charging process, which increases the charging voltage of Battery A. Afterwards, Battery A and B continue to charge up until fully charged.

The variation of SoC has also been taken care of in the developed design.

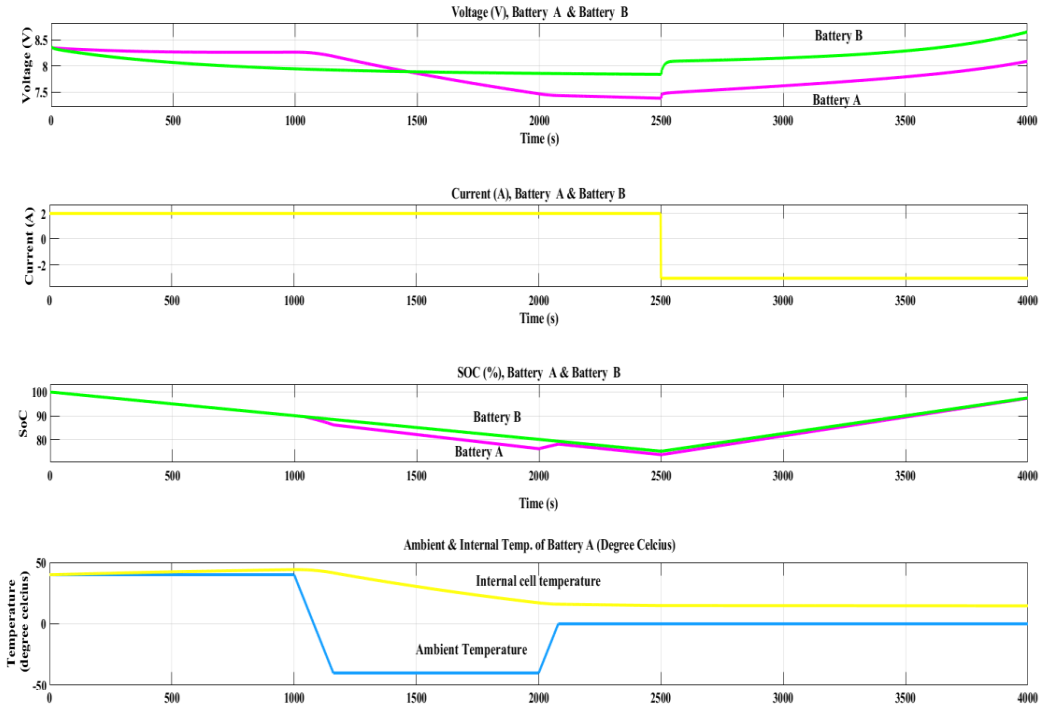

Fig. 3.1.15 Effect of temperature on SoC and voltage of battery A and battery B

3.1.6. Hardware setup and Real-time results

Real-time is often used to describe the time-critical technology in various industries. MicroLabBox uses real-time in reference to an embedded system. These systems are devices which interface with the real world and provide control. The embedded device is given a pre-set time, like 1,5,20 ms to read input signals, to perform all necessary calculations and to write all outputs. The interval size is known as the step size, Ts. Fixed-

step solvers solve the model at regular time intervals from the beginning to the end of the simulation.

Physical test system setups are large, costly, and required highly experienced people to handle the repetitive occupations of setting up networks and maintaining extensive inventories of difficult hardware. With the improvement of microprocessor and floating-point digital signal processing technologies, physical test systems have been replaced with completely real-time simulator. The HEVs are highly non-linear and complex in nature, and testing on the actual network is very expensive, tedious, and risky. Hence, a speedier approach to test and validate a new algorithm or research in a real-world environment using real-time simulator is an essential part of the design and improvement of the system.

There are various types of real-time simulator; the popular real-time platforms are Opal-RT, Typhoon HIL, and MicroLabBox (d-SPACE). In this work, authors have used MicroLabBox hardware controller.

The laboratory setup of HIL has been presented in Fig. 3.1.16 (A). The whole system has been simulated in the MATLAB, and then it is burnt in the MicroLabBOX to verify the results obtained in real-time. The waveform in Fig. 3.1.16 (B) shows two different lines corresponding to two SoCs. The blue line is the SoC due to the original battery (without RC) and the yellow line shows the ANFIS optimized SoC of the 3-RC circuit. The results obtained on the HIL platform are in line with the simulated results. Further, the results obtained using ANFIS based algorithm is very close to the real data, thus verifies the proposed design. In the MicroLabBox it is difficult to show the exact waveform as the signal division is quite large and digital storage oscilloscope (DSO) can only display till M 50s the signal magnitude is further divided by 100 so that it can be stepped down and can be displayed in DSO in real-time. The MATLAB file needs to undergo some setting like fixed solver is selected, step time needs to be fixed and will have to be kept the same for the whole system.

In figure 3.1.16(B) the original SoC indicates the default SoC of the battery i.e battery without any modification which is indicated by the blue line and the SoC of the battery with ANFIS with the 3-RC and has been indicted by the yellow line which runs parallel to blue line but lesser in magnitude. The result shown in 3.1.16(B) is only for 500s as the sampling time of the DSO is 50s so in display at a time in one screen it can show the result for 500s.

A) Hardware setup for the HIL implementation

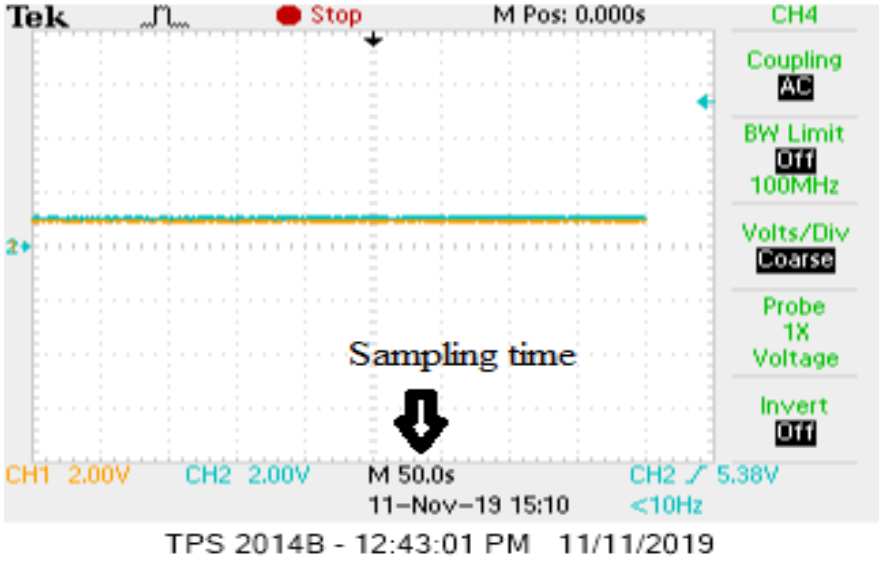

B) SoC versus Time graph (blue line: original SoC, yellow line ANFIS based SoC

Fig. 3.1.16 A) Hardware setup and B) SoC comparison.

3.1.7. Summary

An accurate SoC estimation involving parameter optimization for an HEV. In this work whole battery system of 420V has been considered instead of a single cell. 3-RC pairs are included in the circuit in series with the internal resistance which has produced realistic results for HEV applications. The values of the parameters have been calculated

mathematically and then installed in the circuit to find the new SoC from the modified battery. The obtained parameters are then optimized to get accurate results. To get a precise estimation, this estimated SoC was compared with real data and error was minimized using ANFIS based. The system has been tested on HIL platform by applying MicoLabBox hardware controller. The HIL results are very close to the simulated results.

3.2 Sizing of hybrid energy storage system

3.2.1 Introduction

The performance of any type of EV (XEV) is highly dependent on the ESS (battery) which is a very costly component [119]. The stored energy must be retained for a prolonged period and should be made available at the driver's will. The ESS should be able to get charged and discharged multiple times with great ease without its life degradation. The uptime of the storage must be very high between the replacements, which means that the required mileage of the storage should be very high. Traditionally the electricity was stored in lead-acid batteries [190], [229]–[231]. Though many new types of batteries like ammonia-based batteries, hydrogen fuel cells, and methanol-based batteries are currently under development [232]–[235], but most electric car manufacturers currently prefer to employ Li-ion batteries. These Li-ion batteries get charged quickly, discharged as and when required, deliver high energy to storage ratio, and can satisfy substantial power requirements.

The battery management system (BMS) actively manages the voltage and current of batteries to keep them in the pre-defined limits. Active and passive balancing are essential processes carried out by BMS [236]–[240]. The batteries of EVs can be charged from the wall outlets and by the power generated during regenerative braking. Regenerative braking is a complex mechanism, which produces power while braking the vehicle[241]. Braking does not occur frequently, but whenever it happens, it will produce massive power per unit time, i.e., a considerable amount of energy will be pushed directly into the batteries in a short time. Similarly, during peak traffic period (a common start-stop scenario), there is a high battery discharge in a short interval of time at each start of the vehicle. Both scenarios can lead to damage of the battery chemical properties. The frequent start-stop situations are not suitable for good battery health [242]–[244] and are known to age the battery faster [245], [246]. Degrading SoH presents problems in SoC estimation [247].

There is a crucial need to deploy a device with batteries which can get charged/discharged very quickly, virtually for infinite times. This makes the energy storage a hybrid storage. Additionally, this device should have a high-power dissipation as well as absorption capacity per unit mass. The UCs are well suited for these kinds of applications [248]–[250]. These specific types of capacitors have a very different chemical design than the traditional capacitors. The capacitance values of UCs vary from some farads to tens of hundreds of farads. They can absorb and discharge a large amount of charge in a brief period and can do this frequently for extended periods. The energy-power characteristics of various storages are given in the Ragone plot (Fig. 3.2.1). The high-power density of UCs and high energy density of Li-ion batteries can be combined to improve the performance of existing HESS. Several topologies to design a HES are presented in literature and can be classified into two major categories [251].

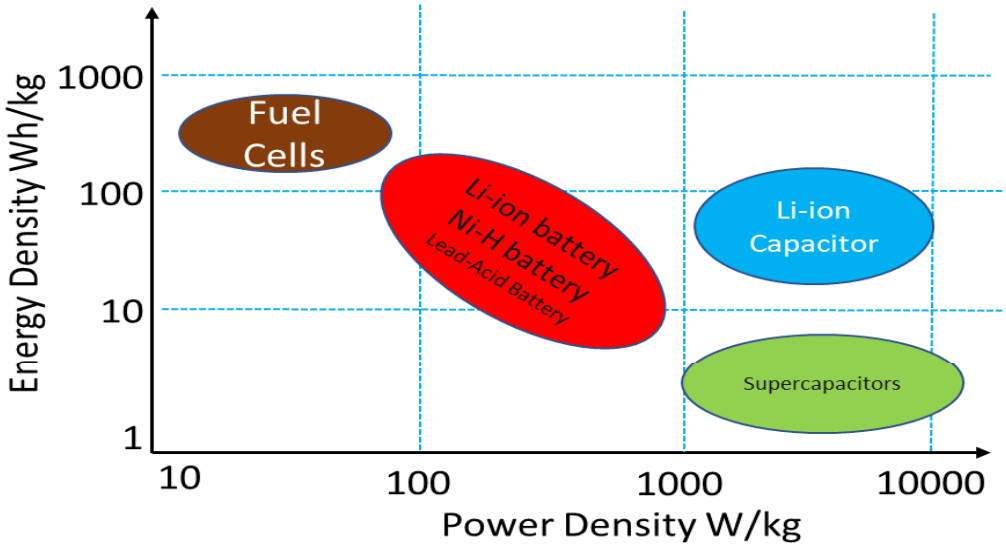

Fig. 3.2.1 Ragone plot of various storages devices [252]

These categories, namely passive HES (P-HES) and active HES (A-HES), are defined based upon the number of power electronics devices used. The categorization also illustrates the level of energy control and optimization in individual elements of the HESS. In a typical P-HES, various energy storage devices are connected in parallel to load without any power electronic decoupling between them. In such cases, due to the significant differences in the charging and discharging curves of the various storage elements, proper optimization is not possible. All the fluctuations in load voltages pass directly to the storage devices degrading the battery life. Therefore, the inclusion of power electronic devices is necessary to reduce the fluctuations reaching to battery modules.

The level of control and optimization in A-HES depends on the number of DC-DC converters included. A-HES is further classified as, semi-active (SA-HES), and fully active (FA-HES). SA-HES topology employs only one DC-DC converter. When this converter is connected before all the parallel-connected storages, voltage fluctuations of UCs will be same as that of battery hence, this scheme (parallel SA –HES or PSA-HES) is not a very

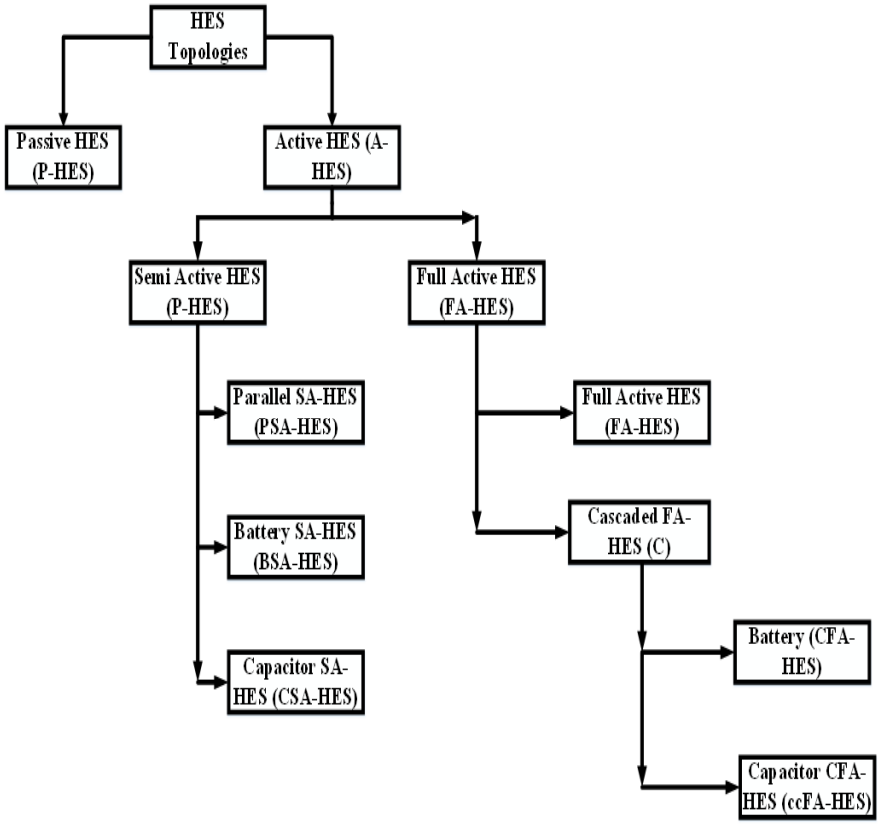

Fig 3.2.2 HES topologies (Zimmermann et al., 2016)

good improvisation over the P-HES. Battery SA-HES (BSA-HES) and capacitor SA-HES (CSA-HES) are further improvisations over PSA-HES. BSA-HES has a DC-DC converter for the battery while CSA-HES has a DC-DC converter for the capacitor. Both topologies aim to restrict the fluctuations due to one storage on the other. But, in both these connections, one of the storage devices remain in direct contact with the load which results in high fluctuation so there is further scope for improvement.

FA-HES better controls the energy flow as compared to SA-HES and can optimize power through each device. FA-HES consists of two main topologies which can be differentiated based on the arrangement of multiple DC-DC converters with respect to each other. Cascaded FA-HES (CFA-HES) has two or more DC-DC converters connected in parallel

to each other. In battery CFA-HES (BCFA-HES) topology, the UCs are decoupled from DC-DC converter, and the battery is further decoupled from UCs using another DC-DC converter. Conversely, in capacitor CFA-HES (CCFA-HES) topology, the batteries are decoupled from the load with a DC-DC converter. Then capacitors are decoupled with batteries by another DC-DC convertor. In these CFA-HES topologies, one of the used storages controls the voltage of the load, and the other tries to follow this voltage. Parallel FA-HES (PFA-HES) is another topology in which all the storage devices are decoupled from the load using separate DC-DC converters. The number of DC-DC converters is directly proportional to the number of separate storage devices used in PFA-HES. The advantage of PFA-HES over CFA-HES is the requirement of simpler DC-DC converters and better control of the energy flow.

Increasing requirement of storage voltage in EVs, requires to create standard battery and UC modules. These modules can be combined in different ways to create larger storages. This creates a requirement of a specialized EMS with dedicated converters for each energy storage device. In the proposed method, a series-parallel FA-HES is discussed. A DC-DC converter is used along with each parallel combination of UC and battery modules to provide a stable voltage to DC voltage line. This article describes a linearly expandable method of using UCs in a hybrid series-parallel combination. The UCs decrease the peak power absorbed and dissipated from the battery modules and hence save the batteries from degrading. This article proposes an EMS, which combines BMS and current management system.

3.2.2. Proposed Methodology

The main aim of the proposed method is to limit the peak absorption and dissipation of the Li-ion batteries to a predefined limit given by the manufacturer to avoid battery health degradation. The value can be updated in the EMS as per the manufacturer or based on other parameters concerning the battery health. This part illustrates the circuit layout and the component specifications of the proposed scheme, after which the simulation environment is portrayed, followed by the parameter estimation and EMS description.

3.2.2.1 Circuit Layout

The proposed method includes battery modules placed in series with each other in voltage additive polarity (Fig. 3.2.3). One UC module is connected in parallel to each battery module, aiming to nullify local above-average peaks in the currents of the individual

battery modules. Another UC module is connected across the circuit, to eliminate any leftover peaks in the load current. Here, assuming almost constant voltage to the load with the help of EMS, the model will consider the load power requirement/supply as a direct function of current passing through the battery. The model will then limit the current through the batteries if it goes above the threshold value in any direction**.**

3a.2.2 Environment for software, hardware, and real-time simulations:

The driving cycle used here is "Indian Driving Cycle" as depicted in Fig. 3.2.4 [253]. The proposed strategy is simulated in the MATLAB environment using Simulink and Simscape Tools. To validate the sanctity of any method, its real rime validation is a must. The HEVs are highly non-linear and complex in nature. Due to lack of financial resources as well as tedious and risky nature of physical test setups, the team chose to use the real-time FPGA and embedded system based MicroLabBox testing setup. It leverages the power of different microprocessors and floating-point digital signal processing technologies present today. The proposed methodology is simulated in MATLAB and then validated in real-time using

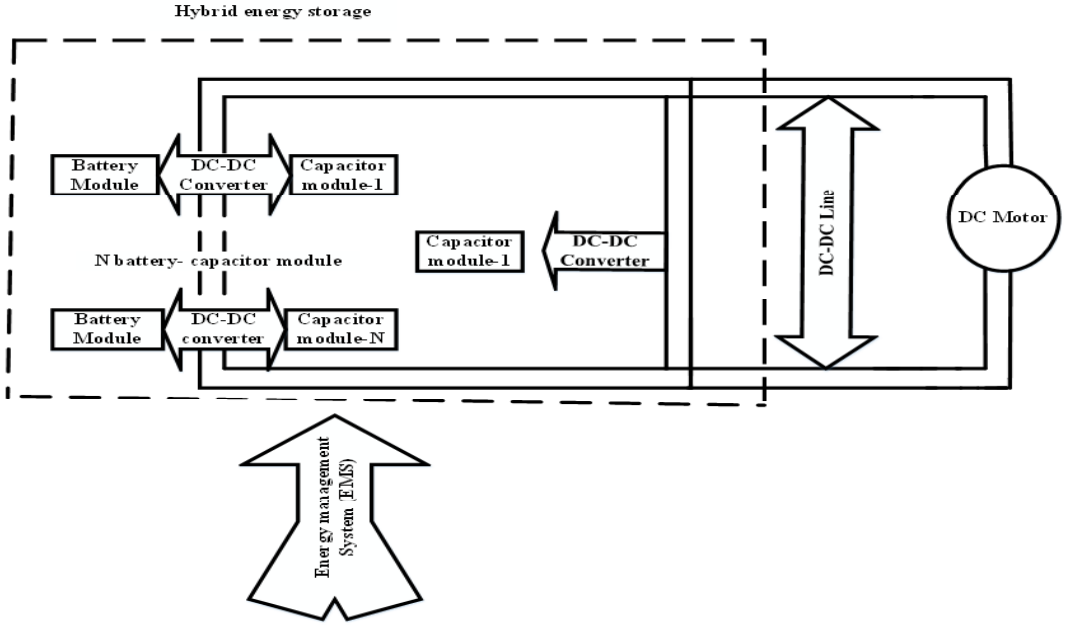

Fig. 3.2.3 Voltage level at different components.

hardware in loop (HIL) testing setup as shown in Fig. 3.2.5. The MicroLabBox has a vertical resolution of only 10 volts, hence the exact waveform of signals with large amplitude cannot be displayed directly. Therefore, the signal magnitude is further divided by 100 to step it down to display on DSO in real-time. Figure 3.2.4 represents the power requirements of the driving cycle, with current requirements and its real-time replica for

the first 500s in Fig. 3.2.6. The replica shown is only for 500s which is the time range limit of the DSO. The oscilloscope provides results of the validation runs.

A finitely chargeable battery model is used in the simulation, which comprises of a series internal resistance and a charge dependant voltage source defined by $V = V_{nominal}*SoC/(1-beta*(1-SoC))$. The beta coefficient is decided by the total chargeable capacity. The UC model used, has a system/combination of a voltage-dependent capacitor with series resistors and capacitors. These parameters were provided based on the actual values of the UCs available in the market.

3.2.2.3 Battery and capacitor specifications*:*

The $LiFePO_4$ Li-ion cells are used in series and parallel combinations to create a battery module. These modules will be capable of supplying the current through parallel combination while simultaneously providing the given voltage due to series connections, hence supplying enough energy for a driving cycle. Similar is the case for the UC cell.

Table 3.2.1 depicts all the specifications.

3.2.2.4 Linearization and sizing of the HES system:

The proposed method helps to find the specifications of components required to design a multiple capacitor-battery (HES) system sufficing the highest peak requirements. A novel approach was needed because the capacitors can only store a small amount of energy but deliver/absorb power at a high rate. While the batteries can store a high amount of energy but cannot deliver/absorb power at a high rate. The linearization method defines the minimum number of Li-ion/UC cells required to form a single module, given the internal resistance and voltage rating of an individual cell. For proper torque, the power requirements should also be known beforehand to decide the number of modules of both

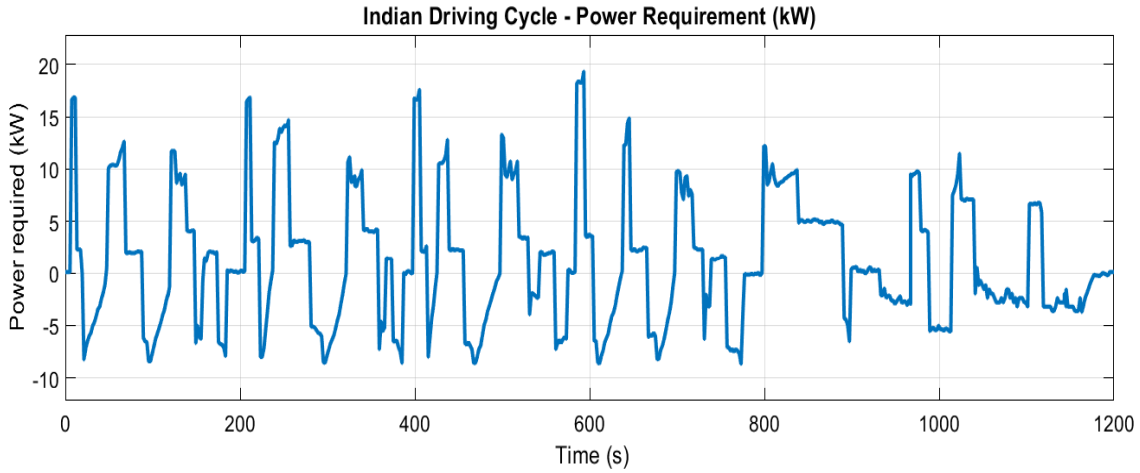

Fig. 3.2.4 Indian driving cycle - power requirements

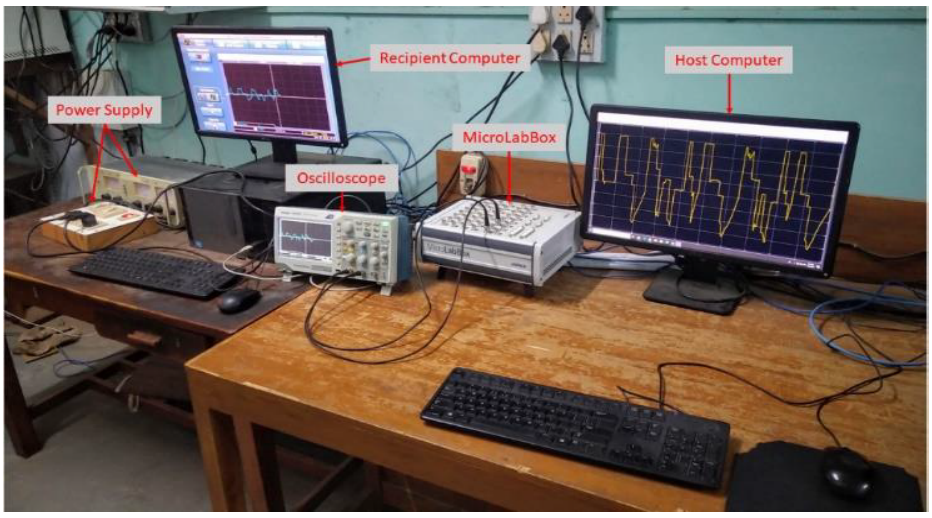

Fig. 3.2.5 Simulation and real-time testing equipment Setup

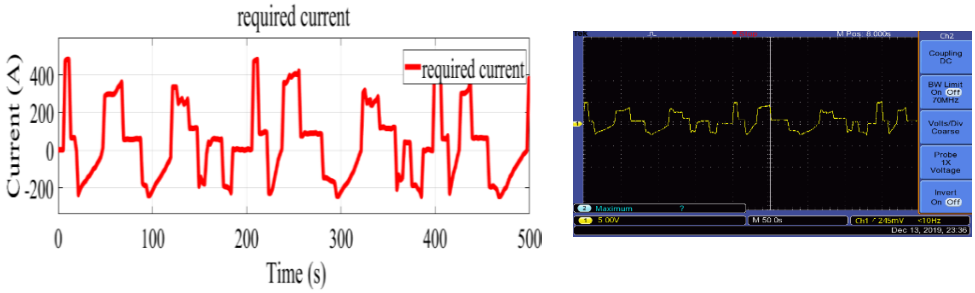

(a) Simulated required current

(b) HIL results of required current

Fig. 3.2.6 Current requirement of the driving cycle (0 – 500s)

capacitors and batteries. The derived voltage value for each module will determine the number of individual cells in series and parallel combination. The specification of the $LiFePO_4$ and UC cell has been provided in Table 3.2.1 -1 (Appendix 1).

Table 3.2.1 Specifications of $LiFePO_4$ and UC cell [254]–[256]

Specifications	LiFePO4 Cell	UC cell	Units
Nominal Voltage	3.3	2.7	V
Nominal Capacity	2.5	N.A.	Ah
Internal Resistance	6	0.29	mΩ
Weight	0.076	0.51	Kg
Rated Capacitance	N.A.	3000	F
Energy Storage	8.25	3.04	Wh
Max. Charge Current	2200	1900000	mA
Max. discharge Current	5200	100000	mA

3.2.2.4.1. Sizing of battery module:

This article designs a generic 48V, 14kWh, and 292 Ah battery, made of 3.3V $LiFePO_4$ cells. For a battery module, the specifications in Table 3.2.1 decides the number of cells in series and parallel.

$$N_{BS} = \frac{V_{BM}}{V_{Li-cell}} \tag{3.2.1}$$

Therefore, at least 16 cells are placed in series into each module of 48V, which accounts for the voltage drop across the internal resistances and interconnects. The current capacity of the module is the next parameter to be considered which needs to be 292Ah. For a single $LiFePO_4$ cell at 3.3V, the energy stored at a safe level is 8.5Wh.

$$\text{Current rating (for one hour)} = \frac{W_{Li\text{-}cell}}{V_{Li\text{-}cell}} \tag{3.2.2}$$

The safe limit of the maximum current considered here is 2A.

$$N_{BP} = \frac{I_{BM}}{I_{Li-cell}} \tag{3.2.3}$$

Hence, each module will have 146 cells in parallel.

$$\text{Total number of cells} = N_{BP} \times N_{BS} \tag{3.2.4}$$

A total number of cells per module comes out to be 2336. The net resistance of the module should also be known to simulate the design accurately. The rated internal resistance of each $LiFePO_4$ cell is 6 mΩ per cell.

Net resistance per battery module = $\frac{N_{BS}}{N_{BP}} \times R_{int}$ (3.2.5)

The net resistance calculated for the given specifications is 0.66 mΩ of each battery module. This value is minimal due to the high number of parallel connections. The graph in Fig. 3.2.4 represents the Indian driving cycle on a 48V battery where maximum power requirement goes about 14kWh. But for safe operation within limits, battery modules must be clipped from the discharging after 90% of the nominal power capacity is dissipated. This limits the batteries to provide only 12.5kWh of the 14kWh storage capacity. As the dynamics of the vehicle will change according to the road conditions and terrain, an upper limit for real-life scenarios must be given, or else the EMS would not be able to properly manage the battery in cases of severe load conditions and very demanding drivers. The safe limits chosen takes into consideration that the threshold values should be less than that. While all the above-mentioned values are in nominal terms, to extend the battery life, the voltage of batteries must remain in the 20% to 80% of nominal voltage values. The value of SoC is hence normalized between the operating (20% - 80% of nominal) battery voltages and is used through the rest of the article. Suppose for the given vehicle design, a net of 140 V is required across the total batteries. It means that 3 individual battery modules, each of 48V, in series combination would be enough to provide 140V. The power requirement and the threshold limits will also be linearly multiplied by 3.

3.2.2.4.2. Sizing of the capacitor module:

As per the proposed strategy, we need to design two different capacitor modules, one for placing in parallel of every individual battery module and the other for putting across the series combination of all the battery modules. All the capacitors will charge and discharge very quickly and change the voltage rapidly across its terminals. A DC-DC bidirectional converter placed at every connection of the capacitor module prevents the battery modules from getting impacted by the voltage fluctuations.

The UCs are rated to work within the voltage fluctuations of 100% to 50% of nominal voltage. The mean of the voltage range of the UC module should be equal to V_{BM} [257].

$$V_{BM} = \frac{V_{UCM} + \frac{V_{UCM}}{2}}{2} \quad (3.2.6)$$

$$V_{UCM} = \frac{4}{3} \times V_{BM} \tag{3.2.7}$$

Equation (3.2.7) results that 62V UC module is required in parallel with each battery module and 186V UC module across the load.

Moving on to the sizing, a 62 V UC module ($C_{int}\ F$) with the minimum safe voltage limit 31V is to be designed. Another UC module ($C_{ext}\ F$), placed across the whole circuit, should be able to handle thrice the voltage values taken for the before mentioned UC module. The maximum voltage for this module will be 62*3, i.e., 186V, and the minimum voltage should be 93V.

Considering that the maximum voltage will appear due to the series combination of the individual UC cell with a nominal voltage of 2.7 volts,

$$N_{UC_{\text{int}}} = \frac{V_{UC_{\text{int}}}}{V_C} \tag{3.2.8}$$

$$N_{UC_{ext}} = \frac{V_{UC_{ext}}}{V_C} \tag{3.2.9}$$

C_1 requires 23 and C_2 requires 79 capacitors cells in series, respectively. Following this, to find the number of UC cells needed in parallel, an analysis of the energy above the safe battery level should be considered. From Fig. 3.2.4, for a 48V battery module, 160500 Ws energy is needed. Therefore, for a 140V configuration, 481500 Ws of energy will be required. The energy requirement values are obtained from the integration of power required in the driving cycle.

$$E_{UC} = \frac{1}{2}\left(3 \times C_{\text{int}} \times \left(V_{UC_{\text{int}}}{}^2 - \left(\frac{V_{UC_{\text{int}}}}{2}\right)^2\right) + C_{ext} \times \left(V_{UC_{ext}}{}^2 - \left(\frac{V_{UC_{ext}}}{2}\right)^2\right)\right) \tag{3.2.10}$$

$$C_{\text{int}} + 3 \times C_{ext} = 111.34 \tag{3.2.11}$$

Any designer would want to use a capacitor module which can be used for making both C_{int} & C_{ext}. Hence, assuming there are $N_{UC_{ex}}$ & $N_{UC_{int}}$ number of similar UC modules in the external (C_{ext}) and internal(C_{int}) capacitors, respectively. Then, let the number of cells in each of the modules be N. Referring to C_{int}, N can be given a value of 23. As C_{ext} requires 69 cells, $N_{UC_{ex}}$ & $N_{UC_{int}}$ can be 3 and 1, respectively. Hence, the relation between C_{ext} & C_{int} is:

$$\frac{C_{\text{int}}}{3} = C_{ext} \tag{3.2.12}$$

Hence, the values of C_{int} and C_{ext} are 100F and 33.33F, respectively. The capacitors taken into consideration are 3000F, 0.29 mΩ capacitors. Sixty-nine capacitors in series combinations make a 33.33F capacitor module, which brings the net capacitance to 3000/69, i.e., 43.5F. Accounting for the I^2R losses, a capacitor of this value can be very well used instead of creating a separate 33.33F capacitor. Similarly, a 3000/23, i.e., 130F capacitor, can be used instead of making 100F. The total resistance of the 130F capacitor is 0.29 mΩ*23, i.e., 6.67 mΩ and that of 43.5F capacitor is 0.29 mΩ*69, i.e., 20 mΩ. This method applies to any appropriate voltage levels required in various vehicles according to their power requirements. Varying the number of modules will produce a discrete range of output voltages.

3.2.2.5 Current limiting and voltage control:

Voltage and current control are the main parts of any power supply design. This module does the logical part of converting the driver's accelerator actuation to an electrical signal for the motor. In this design, the EMS assumes that the batteries are the central power supply unit of the vehicle, and UC modules are the main power absorbers for the regenerative braking of the vehicle. The UC modules also help to supply above-average requirements of the load. The current drawn from the battery module must be limited to the maximum discharge current level of the module (which is 292A). The capacitors should supply any current that is required above this level unless their voltage level goes below the 31V mark. The battery provides current if the capacitor voltage falls below 50% of the nominal voltage level.

During regenerative braking, as mentioned before, a large amount of current will suddenly flow into the storage unit. The capacitors will handle this current until their voltage goes above the maximum 62V. After this, batteries should absorb any more current supplied to the storage system. The flowchart in Fig. 3.2.7 represents the current limiting and voltage control method. It starts with sensing the UC module's voltage and maintaining it under the given range of 100% and 50%.

Case 1: UC Voltage between 100% and 50% of nominal voltages:

In this case, the UC modules are in the optimal voltage range. The battery provides all the current up to 292A for acceleration, above which the capacitors provide the remaining required current. While regenerative braking, the UC module will absorb the current till the 200A, after which the battery module will absorb the surplus. The threshold values are

calculated based on the number of parallel connections per module and the current capacity of each parallel connection.

Case 2: UC Voltage greater than 100% of nominal voltage:

In this case, the UC modules are on the verge of overcharging. Hence any current from the regenerative braking must not enter the UC module. The battery will absorb all the current from the regenerative braking. The current requirements of the load will be fulfilled, as in case 1.

Case 3: UC Voltage is less than 50% nominal voltage:

In this range, the UC module is undercharged, and will not be able to provide any current. Hence battery will have to supply any amount of current required by the load. The regenerative braking will work the same as in case 1.

3.2.2.6 SoH comparison:

The chemical properties of any battery change over time. The aging occurs due to the various charging and discharging events that take place during the life of the battery. The manufacturer of batteries designs a maximum charge capacity for the batteries. But due to aging over time, the batteries lose some part of this capacity. The remaining capacity of the batteries is inversely proportional to the change in SoC over the observation time interval. Then the SoH of a battery can then be defined as a ratio of residual charging capacity ($C_{residue}$) and specified charging capacity ($C_{Specified}$).

$$C_{residue} \propto \frac{1}{SoC_{t_1} - SoC_{t_2}} \tag{3.2.13}$$

$$SoH = \frac{C_{residue}}{C_{specified}} \tag{3.2.14}$$

To compare different EMS, the ratio of respective SoH can be taken, which will eventually result in an inverse of the ratio of change in SoC due to respective methods over time.

3.2.3. Results and Analysis

The proposed system with identified circuit parameters is simulated in MATLAB and then tested in real-time using MicroLabBox hardware test setup for various operating conditions. In the section below results are presented and analysed. In all the following figures, HIL results are represented by *'H'* and MATLAB simulations are represented by *'S'*, wherever required.

3.2.3.1 Comparison of HES performance with and without regenerative braking:

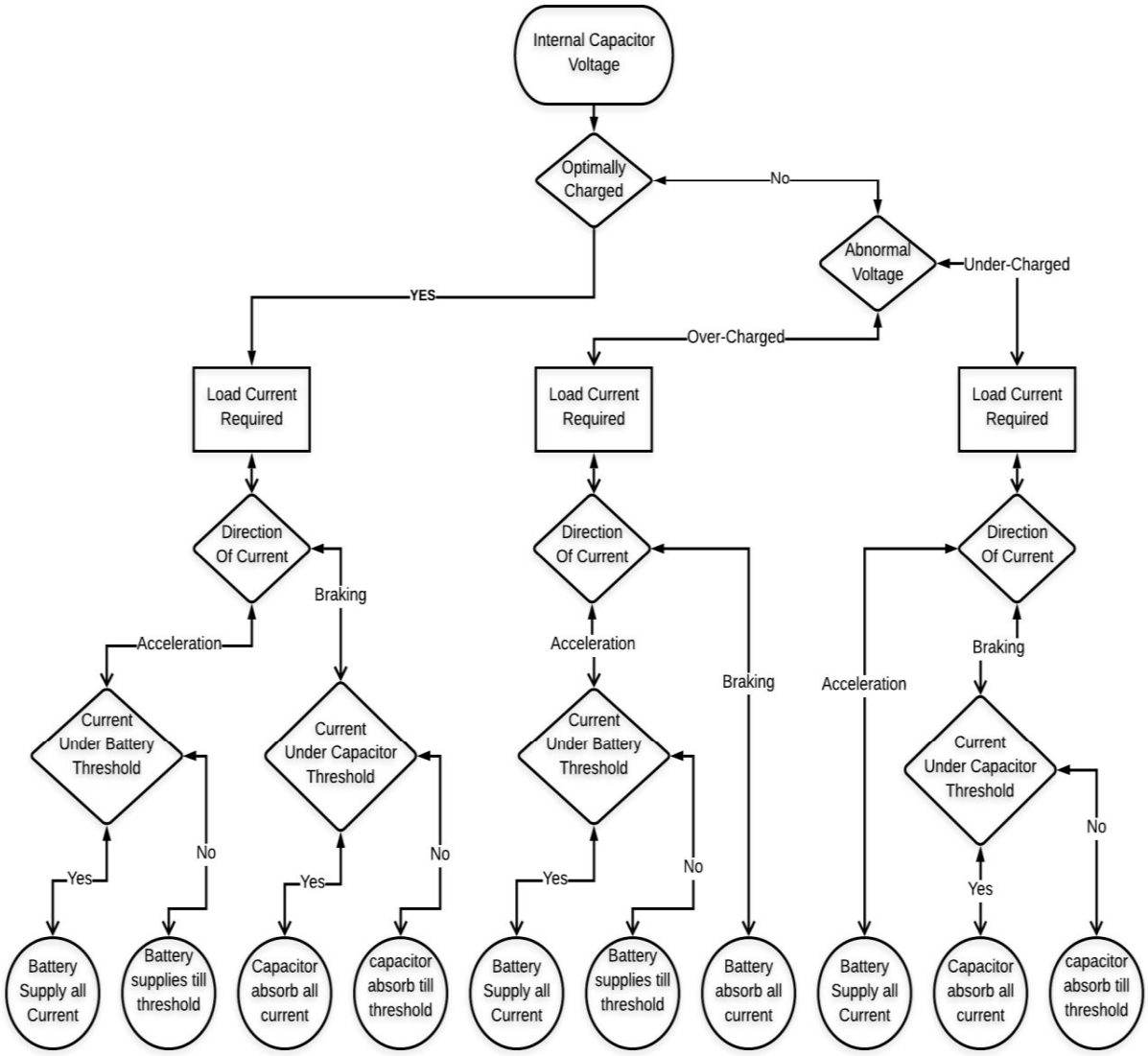

Fig. 3.2.7 Proposed energy management

EMS is not enabled in this case to showcase the effects of regenerative braking. In the absence of regenerative braking, the voltage and hence the charge content of the batteries will deplete faster compared to regenerative braking enabled. When regenerative braking is enabled, net power provided to the vehicle is the addition of power supplied by the batteries and power gained from regenerative braking. As the net power taken by the vehicle is the same for both the cases, the batteries will have to work harder in the case when regenerative braking is not enabled. Hence net fall in the SoC level will be less in case of regenerative braking as observed in Fig. 3.2.8(a). A similar effect on the voltage levels is also observed in Fig. 3.2.8(b).

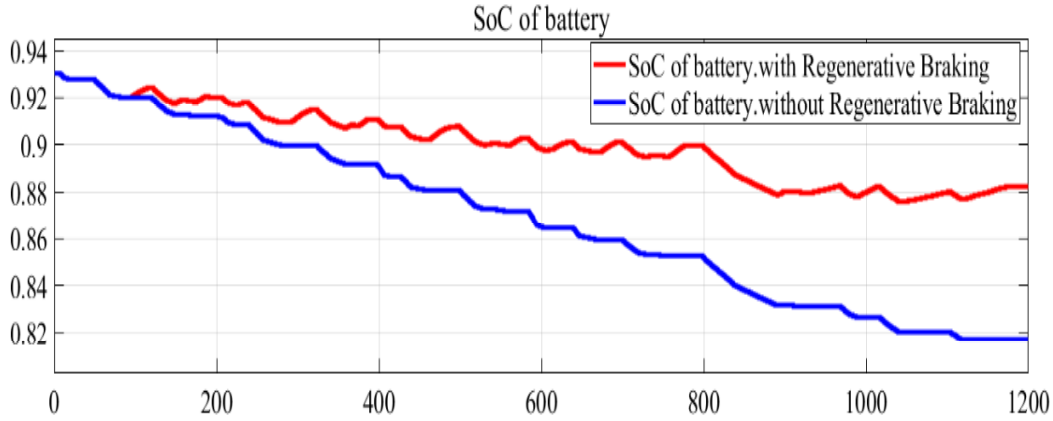

(a) Battery SoC

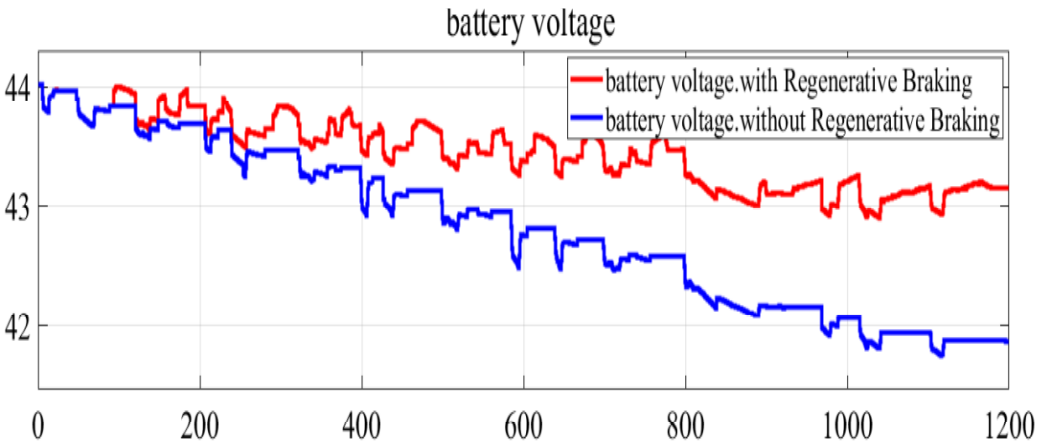

(b) Battery Voltage

Fig. 3.2.8: Battery voltage with and without enabling regenerative braking.

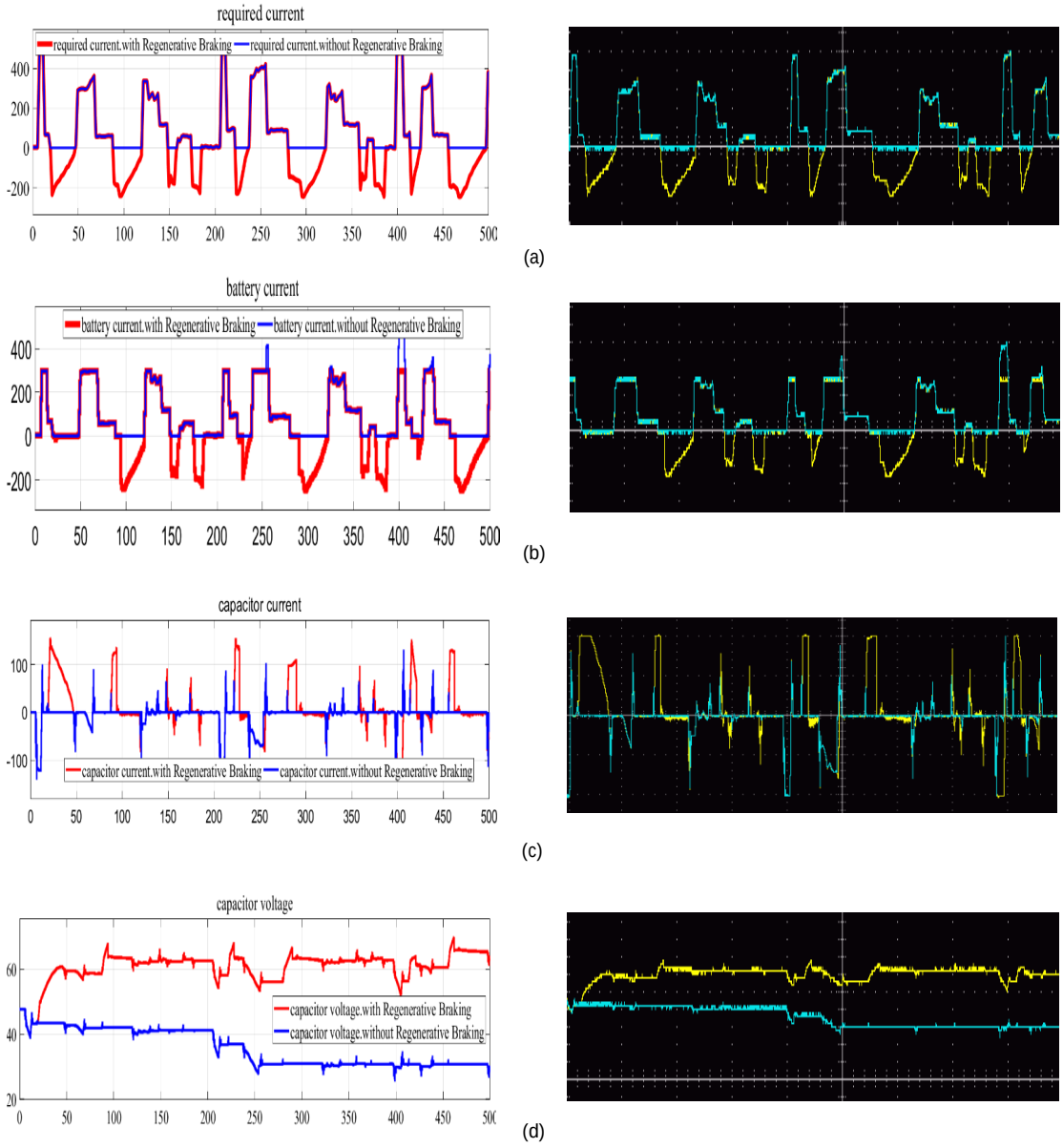

Fig. 3.2.9 HES performance with and without regenerative braking (with real-time results)

Capacitor aided storage modules also show a similar trend. The MATLAB simulation for capacitor aided storages, along with their real-time results for the first 500s are shown in Fig. 3.2.9, displaying the exact correspondence of the current and the voltages of various components. The current through the capacitors with regenerative braking enabled (Fig. 3.2.9(c)) shows positive spikes, conveying that capacitor are charging. The capacitor will stay charged due to frequent braking in the case of regenerative braking enabled, while it would drain to 50% of the nominal voltage level, in the other case (Fig. 3.2.9(d)).

3.2.3.2 Comparison of HES performance with and without using UCs:

EMS is not enabled in this case to showcase the effects of UCs. The use of UC modules is relevant for the proposed method as the aim is to decrease the usage of batteries at high current supply or absorption rates. The energy supplied or absorbed by the capacitors will supplement the batteries in meeting the power requirement of the vehicle.

For a demonstration of this idea, a 48V battery module designed earlier is used in parallel with the 62V capacitor module (Fig. 3.2.10 & Fig. 3.2.11). Figure 3.2.10 provides the insight of the before mentioned idea. The current through batteries is significantly less when capacitors are used while the battery current show huge spikes when used without

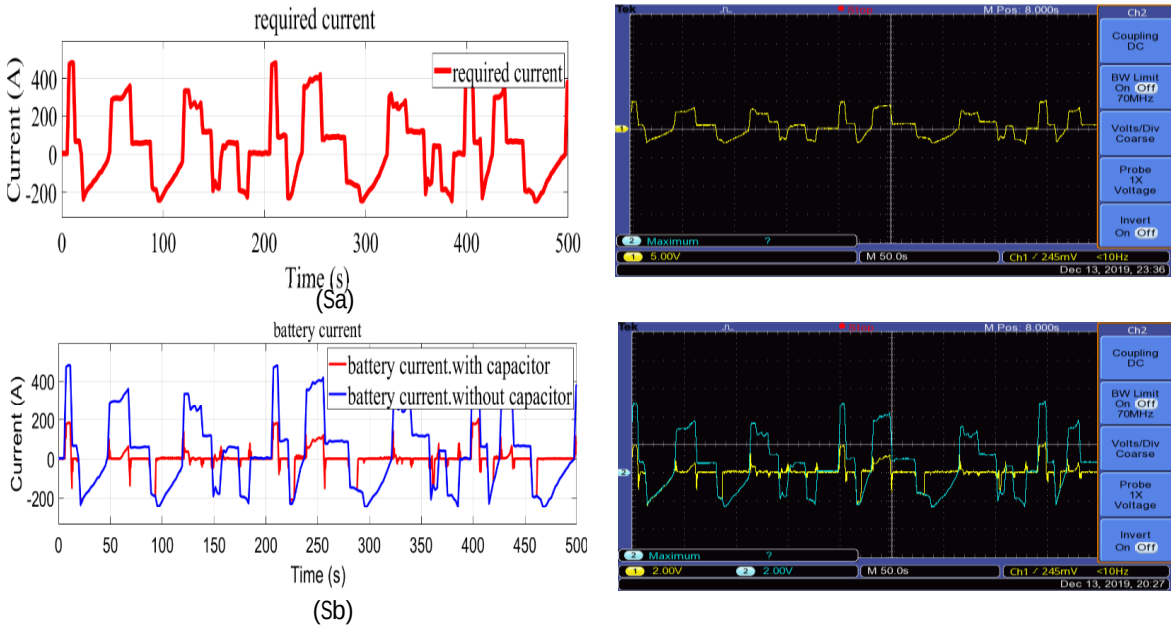

Fig. 3.2.10 Comparison of HES performance with and without ultra-capacitors

capacitors. Similar trends are shown in Fig. 3.2.11(b) representing a repetition of the driving cycle four times. In the case of not using the capacitor and no limits on the discharge & charge current to the battery, it is evident that the battery module is supplying an excess of 400A to the load and absorbing around 200A while regenerative braking scenarios. After using capacitors, the maximum current supplied by the battery limits to under 300A. Similarly, the charging current is also decreased significantly.

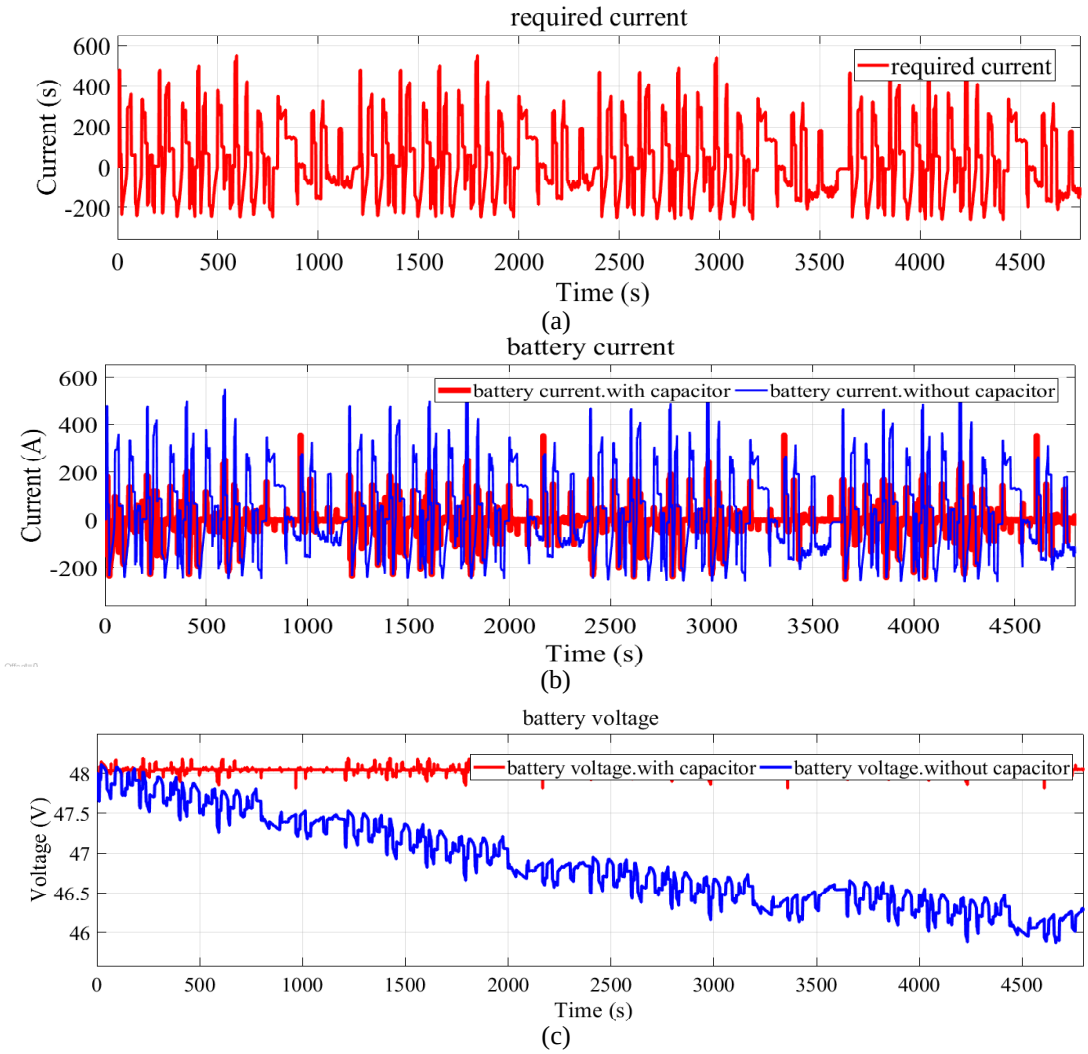

Fig. 3.2.11 Comparison of battery performance with and without ultra-capacitors

These limitations save the batteries from degrading its SoH as well as minimize the voltage fluctuations (Fig. 3.2.11c). The voltage of the battery (Fig. 3.2.11c) enables the reader to visualize the amount of voltage drainage over repetitive driving in the two given scenarios.

3.2.3.3 Simulation of the proposed circuit design:

The proposed method consists of multiple capacitors and battery modules connected, as explained in the "circuit layout" section. The current form of the Indian driving cycle is used for the load (EV) simulation (Fig. 3.2.6 & Fig. 3.2.13a). All the parameters, defined in the "Linearization and Sizing" section as well as the EMS, are applied to the MATLAB components. Fig. 3.2.12 and Fig. 3.2.13 show the power and current fluctuations, respectively, with their real-time HIL results for 500s. The EMS manages current in both directions (Fig. 3.2.13). Any positive current represents current supplied by the storage, while regenerative braking causes the negative flow of current. Here, reconsidering the

facts that were taken care of when designing the battery module, a current limit of 292A is applied to the discharge current of the battery, while the current required above the 292A mark is supplied by the capacitor module. Similarly, a limit of 200A is applied to the charging current of the capacitor, while the excess of which will be readily absorbed by the battery module. Figure. 3.2.13 shows current limiting by the EMS in the proposed method. Then the model is run for the driving cycles repetitively to see the dynamics of the battery voltage over the cycles (Fig. 3.2.14). The voltage is also managed by the EMS (Fig. 3.2.14).

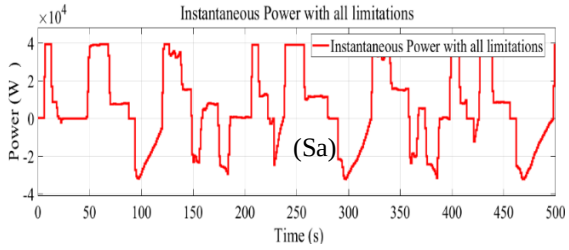

(Sb)

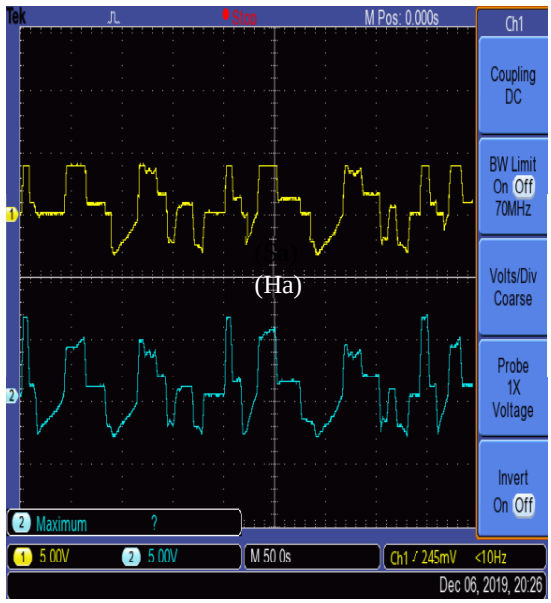

(Hb)

Fig. 3.2.12 Power levels of the battery modules

It shows fewer fluctuations when compared to methods without capacitor modules and EMS. The combination of capacitors and EMS readily removes peaks from the battery module voltages.

The main aim was to limit the power input and output of the battery modules. Limiting current and voltage levels automatically control the power to a safe level, and the capacitor modules will do all the power input and output over and above the safe limits. The power limiting is observable in Fig. 3.2.12. The net power required at any given point in time is the same as in Fig. 3.2.12b, where no capacitors are used. Usage of capacitors as a secondary storage unit for energy limits the power requirements from the battery to a lower level. Fig. 3.2.12a shows the peaks of the required power from the battery are removed and flattened. At the same time, the capacitors provide all the excess requirements.

3.2.3.4 Justification of using multiple converters.

For the analysis, three storages with a different number of converters are chosen. The proposed multiple converters arrangement has been shown in 3.2.14. A comparison of the proposed method and methods with similar storage capacity but a lesser number of converters are provided in Fig. 3.2.15.

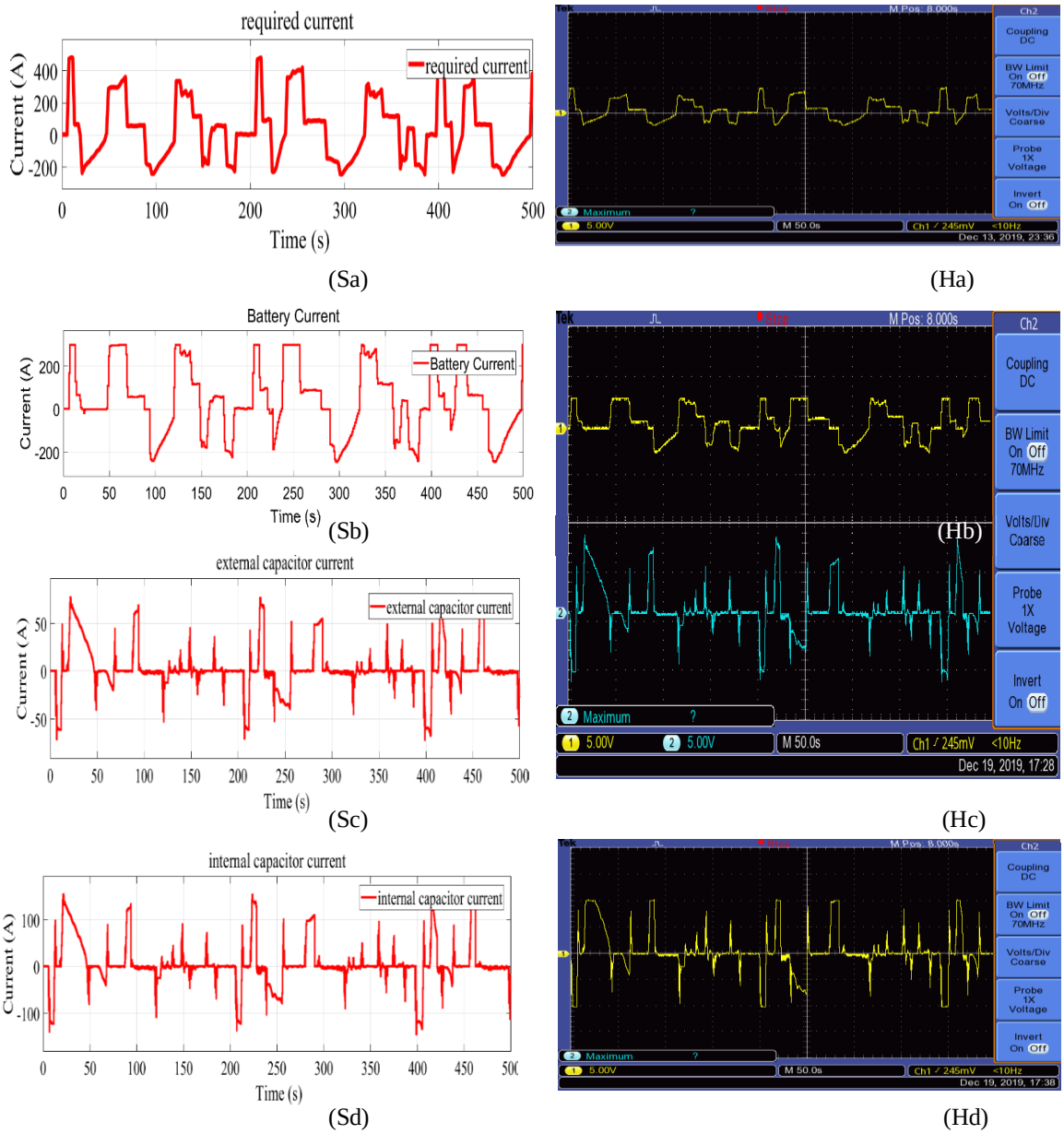

Fig. 3.2.13 Current through various components

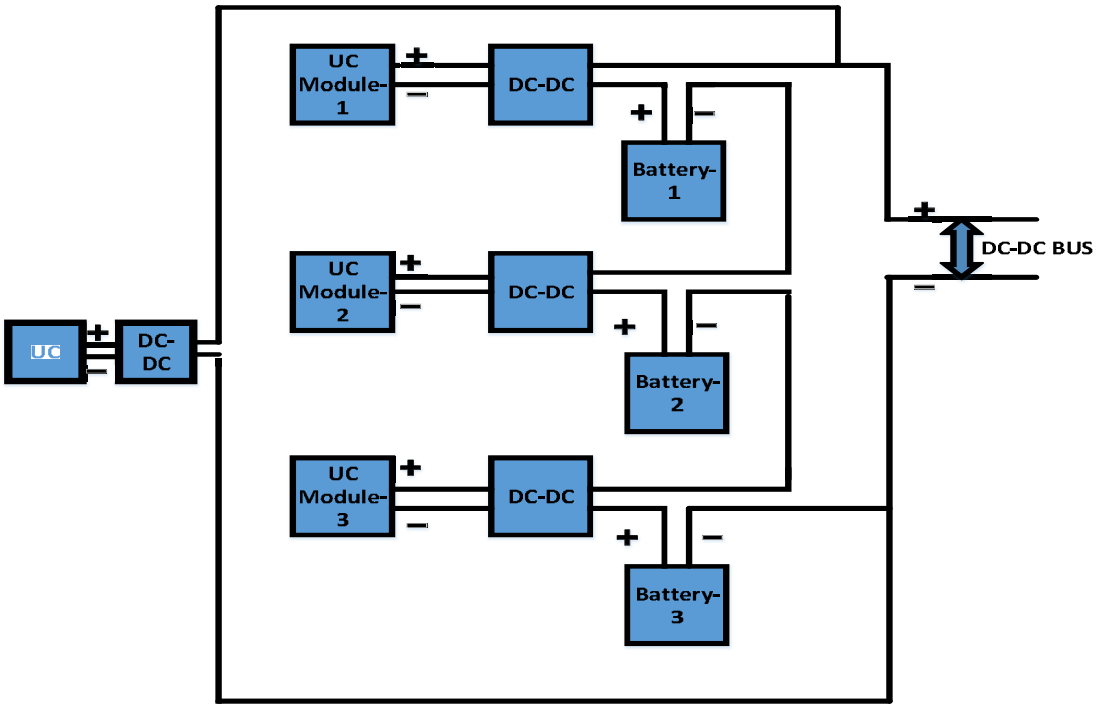

Fig. 3.2.14 Proposed multiple converters arrangement

The three cases compared are as follows: first one is the proposed storage, the second is storage with no external converter across DC bus, and the third storage is without any converter. In all cases, the storages have been charged with a constant 50 A current and then can discharge through a constant load of what rating (internal resistance 10 Ω). From Fig. 3.2.15, it is observable that the proposed storage retains higher and constant SoC levels for a longer time. As the number of converters decreases, the voltage stability decreases, and the SoC levels go down quickly than the proposed method. With the removal of one converter from the proposed storage, the SoC decreases almost 500s earlier. With no converters used, the battery gets overcharged during charging due to the capacitors and then discharges as soon as the load is applied. This proves the effectiveness of multiple smaller converters specific to each module. In the long run, retaining higher levels of battery SoH along with usage of multiple economic converters will save money by increasing the time span between replacements of batteries. The cost of the storage due to the use of multiple low rated converters is almost the same as of a single high rating converter used in BMS. Though the EMS can become complicated, but it provides better conditions for the battery modules.

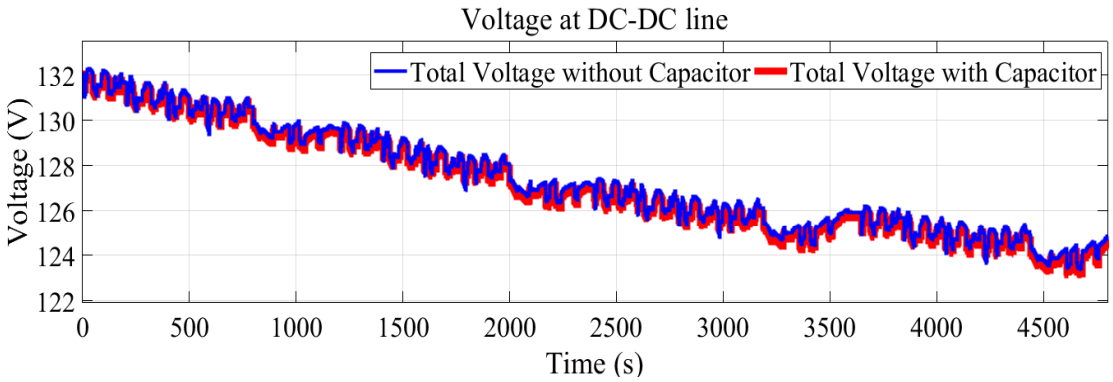

Fig. 3.2.15 Voltage on DC-DC line during four continuous driving

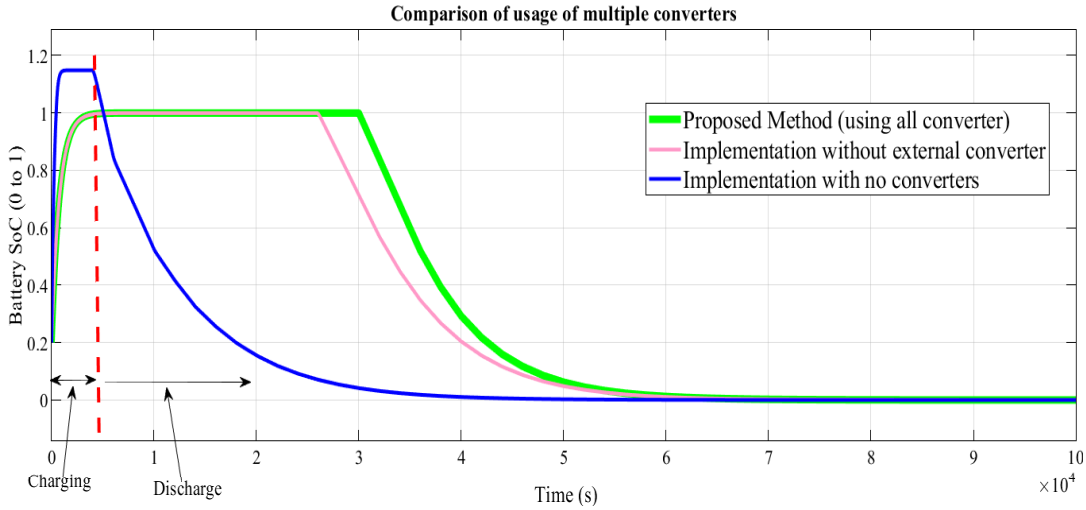

Fig. 3.2.16 Comparison of usage of multiple converters

In the implementation without the usage of converters, the SoC of the battery rises to 1.2 which means that the voltage of the battery is above 80% of nominal value. This indicates that heavy fluctuations in battery voltages when it is charged without proper control.

3a.3.5 Contributions of the proposed method:

The major contributions of the proposed method can be seen from Table 3.2.2 and Fig. 3.2.16 where fluctuations in SoC and its corresponding peak-to-peak values have been decreased. The proposed method provides a boost of 38.6% in SoH over the conventional method. This means that the chemical and physical composition are kept healthier with the help of the proposed method. Therefore, the proposed method makes the battery-less prone to the fluctuations in supplied and absorbed power, saving its health and retaining high SoH which increases RUL of the battery for a given number of the charge/discharge cycles.

Table 3.2.2 SoC comparison of proposed method and conventional method (Fig. 3a.16):

Sr. no.	Time (s)	No. of driving cycles	Conventional method (SoC)	Proposed method (SoC)
1.	0 s	0	0.95	0.95
2.	4800 s	4	0.766	0.838
Difference			0.184	0.113
Peak-to-peak fluctuation			0.1870	0.1229

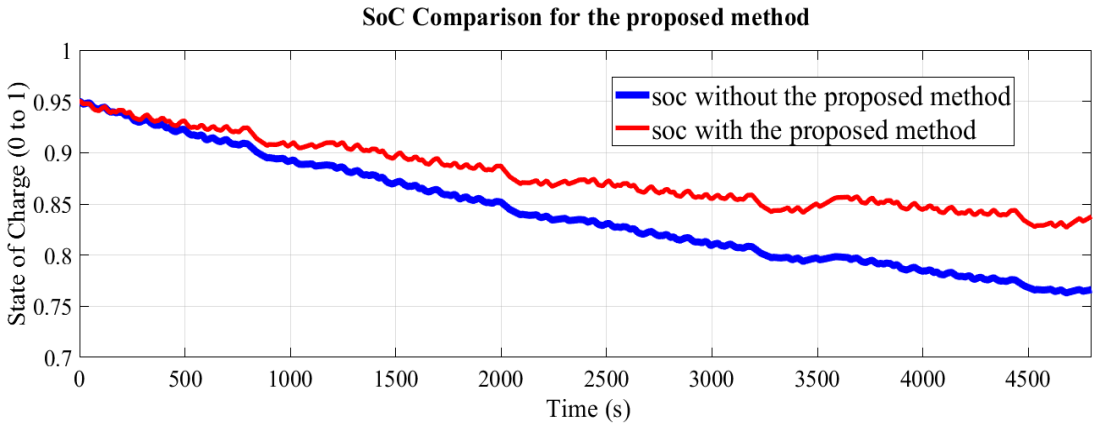

Fig. 3.2.16 SoC Comparison

The proposed approach employs multiple low rated converters which maintain a constant voltage across the batteries and on the DC bus. Further, it enables controlled current discharge from the batteries as well as the capacitors, maintaining similar voltages and temperatures across the storage. Being low voltages and power ratings, their size, weight, cost, and losses are less.

3.2.4. Summary

This chapter presents a HESS wherein UC in conjunction with the Li-ion batteries. The batteries are used as a primary source of power, while UC are used to provide and absorb peak power requirements.

The proposed method reduces frequent significant peaks in the current input and output from the battery, which has been quantitatively proven by higher SoC levels using this scheme than conventional methods. The proposed method also provides better health of battery over several charging and discharging cycles, giving a significant boost to the available mileage of batteries. Improvement of 38.6% in SoH is observed over conventional HESS methods on Indian driving cycle.

The proposed method can also help in the development of sophisticated EMS and can be extended to any driving cycles.